4. Takahashi T, Kalka C, Masuda H, et al. Ischemia- and cytokine-induced mobilization of bone marrow-derived endothelial progenitor cells for neovascularization. *Nat Med.* 1999;5:434–438.
5. Gill M, Dias S, Hattori K, et al. Vascular trauma induces rapid but transient mobilization of VEGFR2(+)AC133(+) endothelial precursor cells. *Circ Res.* 2001;88:167–174.
6. Kawamoto A, Gwon HC, Iwaguro H, et al. Therapeutic potential of ex vivo expanded endothelial progenitor cells for myocardial ischemia. *Circulation.* 2001;103:634–637.
7. Tabata Y, Nagano A, Ikada Y. Biodegradation of hydrogel carrier incorporating fibroblast growth factor. *Tissue Eng.* 1999;5:127–138.
8. Fukunaka Y, Iwanaga K, Morimoto K, et al. Controlled release of plasmid DNA from cationized gelatin hydrogels based on hydrogel degradation. *J Control Release.* 2002;80:333–343.
9. Tabata Y, Ikada Y. Macrophage activation through phagocytosis of muramyl dipeptide encapsulated in gelatin microspheres. *J Pharm Pharmacol.* 1987;39:698–704.
10. Owji AA, Smith DM, Coppock HA, et al. An abundant and specific binding site for the novel vasodilator adrenomedullin in the rat. *Endocrinology.* 1995;136:2127–2134.
11. Yoshibayashi M, Kamiya T, Kitamura K, et al. Plasma levels of adrenomedullin in primary and secondary pulmonary hypertension in patients <20 years of age. *Am J Cardiol.* 1997;79:1556–1558.
12. Nagaya N, Satoh T, Nishikimi T, et al. Hemodynamic, renal and hormonal effects of adrenomedullin infusion in patients with congestive heart failure. *Circulation.* 2000;101:498–503.
13. Nagaya N, Nishikimi T, Uematsu M, et al. Haemodynamic and hormonal effects of adrenomedullin in patients with pulmonary hypertension. *Heart.* 2000;84:653–658.
14. Murohara T, Ikeda H, Duan J, et al. Transplanted cord blood-derived endothelial precursor cells augment postnatal neovascularization. *J Clin Invest.* 2000;105:1527–1536.
15. Kalka C, Masuda H, Takahashi T, et al. Vascular endothelial growth factor (165) gene transfer augments circulating endothelial progenitor cells in human subjects. *Circ Res.* 2000;86:1198–1202.
16. Dimmeler S, Aicher A, Vasa M, et al. HMG-CoA reductase inhibitors (statins) increase endothelial progenitor cells via the PI 3-kinase/Akt pathway. *J Clin Invest.* 2001;108:391–397.
17. Kalka C, Masuda H, Takahashi T, et al. Transplantation of ex vivo expanded endothelial progenitor cells for therapeutic neovascularization. *Proc Natl Acad Sci U S A.* 2000;97:3422–3427.
18. Priller J, Flugel A, Wehner T, et al. Targeting gene-modified hematopoietic cells to the central nervous system: use of green fluorescent protein uncovers microglial engraftment. *Nat Med.* 2001;7:1356–1361.
19. Rosenberg H, Rabinovitch M. Endothelial injury and vascular reactivity in monocrotaline pulmonary hypertension. *Am J Physiol.* 1988;255:H1484–H1491.
20. Horio T, Kohno M, Kano H, et al. Adrenomedullin as a novel antimigration factor of vascular smooth muscle cells. *Circ Res.* 1995;77:660–664.

Am J Physiol Heart Circ Physiol 285: H2125–H2131, 2003;
10.1152/ajpheart.00548.2002.

Repeated inhalation of adrenomedullin ameliorates pulmonary hypertension and survival in monocrotaline rats

Noritoshi Nagaya,[1] Hiroyuki Okumura,[2] Masaaki Uematsu,[3] Wataru Shimizu,[1] Fumiaki Ono,[1] Mikiyasu Shirai,[4] Hidezo Mori,[4] Kunio Miyatake,[1] and Kenji Kangawa[2]

[1]*Department of Internal Medicine, National Cardiovascular Center, Osaka 565-8565;*
[2]*Department of Biochemistry, National Cardiovascular Center Research Institute, Osaka 565-8565;*
[3]*Cardiovascular Division, Kansai Rosai Hospital, Hyogo 660-0064, Japan; and* [4]*Department of Cardiac Physiology, National Cardiovascular Center Research Institute, Osaka, Japan 565-8565*

Submitted 1 July 2002; accepted in final form 31 December 2002

Nagaya, Noritoshi, Hiroyuki Okumura, Masaaki Uematsu, Wataru Shimizu, Fumiaki Ono, Mikiyasu Shirai, Hidezo Mori, Kunio Miyatake, and Kenji Kangawa. Repeated inhalation of adrenomedullin ameliorates pulmonary hypertension and survival in monocrotaline rats. *Am J Physiol Heart Circ Physiol* 285: H2125–H2131, 2003; 10.1152/ajpheart.00548.2002.—Adrenomedullin (AM) is a potent vasodilator peptide. We investigated whether inhalation of aerosolized AM ameliorates monocrotaline (MCT)-induced pulmonary hypertension in rats. Male Wistar rats given MCT (MCT rats) were assigned to receive repeated inhalation of AM ($n = 8$) or 0.9% saline ($n = 8$). AM (5 μg/kg) or saline was inhaled as an aerosol using an ultrasonic nebulizer for 30 min four times a day. After 3 wk of inhalation therapy, mean pulmonary arterial pressure and total pulmonary resistance were markedly lower in rats treated with AM than in those given saline [mean pulmonary arterial pressure: 22 ± 2 vs. 35 ± 1 mmHg (−37%); total pulmonary resistance: 0.048 ± 0.004 vs. 0.104 ± 0.006 $mmHg \cdot ml^{-1} \cdot min^{-1} \cdot kg^{-1}$ (−54%), both $P < 0.01$]. Neither systemic arterial pressure nor heart rate was altered. Inhalation of AM significantly attenuated the increase in medial wall thickness of peripheral pulmonary arteries in MCT rats. Kaplan-Meier survival curves demonstrated that MCT rats treated with aerosolized AM had a significantly higher survival rate than those given saline (70% vs. 10% 6-wk survival, log-rank test, $P < 0.01$). In conclusion, repeated inhalation of AM inhibited MCT-induced pulmonary hypertension without systemic hypotension and thereby improved survival in MCT rats.

vasodilator; hemodynamics; aerosol; survival

ADRENOMEDULLIN (AM) is a potent vasodilator peptide that was originally isolated from human pheochromocytoma (13). Immunoreactive AM has subsequently been detected in plasma and a variety of tissues, including blood vessels and the lungs (9, 27). It has been reported that there are abundant binding sites for AM in the lungs (24). We (11, 30) have shown that the plasma AM level increases in proportion to the severity of pulmonary hypertension and that circulating AM is partially metabolized in the lungs. Interestingly, AM has been shown to inhibit the migration and proliferation of vascular smooth muscle cells (8, 12). These findings suggest that AM plays an important role in the regulation of pulmonary vascular tone and vascular remodeling.

In fact, experimental studies (5, 14, 22) have demonstrated that intralobar arterial infusion of AM induces pulmonary vasodilation in rats and cats. In humans, we have shown that short-term intravenous infusion of AM significantly decreases pulmonary vascular resistance in patients with congestive heart failure (19) or primary pulmonary hypertension (PPH) (18). Unfortunately, however, intravenously administered AM also decreases systemic arterial pressure in such patients because of its nonselective vasodilation in pulmonary and systemic vascular beds.

Recently, inhaled prostacyclin and its analog, iloprost, have been shown to cause pulmonary vasodilation without systemic hypotension in patients with PPH (7, 28, 29). In addition, the inhalant application of vasodilators does not induce negative side effects on gas exchange, because ventilation-matched deposition of the drugs in the alveoli causes pulmonary vasodilation matched to ventilated areas (28). In clinical settings, inhalation therapy may be more simple, noninvasive, and relatively comfortable than continuous intravenous infusion therapy. These findings raise the possibility that intratracheal delivery of aerosolized AM may have beneficial effects in patients with precapillary pulmonary hypertension.

Thus the purpose of the present study was to investigate whether inhalation of AM ameliorates monocrotaline (MCT)-induced pulmonary hypertension and thereby improves survival in MCT-treated rats.

METHODS

Animals. Male Wistar rats weighing 80 to 100 g were used in this study. The rats were given a subcutaneous injection of 60 mg/kg MCT (MCT rats) and assigned to receive a single inhalation of AM ($n = 5$) or 0.9% saline ($n = 5$) or repeated inhalation of AM ($n = 8$) or 0.9% saline ($n = 8$). Sham rats not

Address for reprint requests and other correspondence: N. Nagaya, Dept. of Internal Medicine, National Cardiovascular Center, 5-7-1 Fujishirodai, Suita, Osaka 565-8565, Japan (E-mail: nagayann@hsp.ncvc.go.jp).

The costs of publication of this article were defrayed in part by the payment of page charges. The article must therefore be hereby marked "*advertisement*" in accordance with 18 U.S.C. Section 1734 solely to indicate this fact.

given a MCT injection also received repeated inhalation of AM (n = 8) or 0.9% saline (n = 8). An additional 20 rats were studied to evaluate the effects of inhaled AM on survival in MCT rats. Finally, rats that had developed pulmonary hypertension 3 wk after the MCT injection received repeated inhalation of AM (n = 8) or 0.9% saline (n = 8). All protocols were performed in accordance with guidelines of the Animal Care Ethics Committee of the National Cardiovascular Center Research Institute (Osaka, Japan).

Preparation of AM. Recombinant human AM was obtained from Shionogi (Osaka, Japan). The homogeneity of AM was confirmed by reverse-phase HPLC and amino acid analysis. AM was dissolved in 0.9% saline, and the solution was stored as 20-ml volumes containing 200 μg AM/tube at −80°C until the time of preparation for administration.

Inhalation of AM. We used an unrestrained, whole body aerosol exposure system. Each rat was placed in a plastic cage for aerosol delivery. AM or saline was aerosolized using an ultrasonic nebulizer (Soniclizer 305, Atom) connected to six cages. The 20 ml solution containing 200 μg AM was delivered as an aerosol into the six cages at a constant flow rate (0.6 ml solution/min) for 30 min. Inhalation of fluorescein isothiocyanate-dextran demonstrated that a single inhalation of AM delivered 0.5 μg AM to the lungs in each rat (5 μg/kg body wt).

To assess the acute effect of inhaled AM, hemodynamic studies were carried out at 3 wk after the MCT injection. Hemodynamics were measured at 15-min intervals before, during, and after a single inhalation of AM or saline. Blood was obtained from the carotid artery at the same time points for measurement of plasma AM.

To assess the chronic effect of inhaled AM, 30-min inhalation of AM (5 μg/kg body wt) or saline was repeated four times a day for 3 wk after the MCT injection. Finally, to investigate the effects of inhaled AM on developed pulmonary hypertension, aerosolized AM or saline was given for 1 wk to rats that had developed pulmonary hypertension 3 wk after the MCT injection. After completion of the inhalation therapy, hemodynamic studies were performed. Blood was then drawn from the carotid artery for measurement of plasma hormone levels. Finally, cardiac arrest was induced by the injection of 2 mmol KCl through the catheter. The ventricles and lungs were excised, dissected free, and weighed. The measurement of right ventricular weight excluded the interventricular septum. The ratio of right ventricular weight to body weight and the ratio of left ventricular weight to body weight were calculated as indexes of ventricular hypertrophy.

Hemodynamic measurements. Rats were anesthetized with intraperitoneal pentobarbital (30 mg/kg) and placed on a heating pad to maintain body temperature at 37–38°C throughout the study. A polyethylene catheter (PE-10) was inserted into the right femoral artery to measure heart rate and mean arterial pressure. An umbilical vessel catheter was inserted through the right jugular vein into the pulmonary artery for the measurement of right ventricular pressure and pulmonary arterial pressure. These hemodynamic variables were measured using a pressure transducer (model P23ID, Gould) connected to a polygraph and recorded with a thermal recorder (7758B system, Hewlett-Packard). A thermomicroprobe was advanced into the ascending aorta via the right carotid artery and connected to a cardiac output computer (Cardiotherm-500, Columbus Instruments). Cardiac output was measured in triplicate by the thermodilution method. Total pulmonary resistance was calculated by dividing the mean pulmonary arterial pressure by the cardiac output.

Morphometric analysis of pulmonary arteries. Paraffin sections 4 μm in thickness were obtained from the middle region of the right lung and stained with hematoxylin and eosin for examination by light microscopy. Analysis of the medial wall thickness of the pulmonary arteries was performed as described previously (23). In brief, the external diameter and the medial wall thickness were measured in 20 muscular arteries (ranging in external diameter from 25 to 50 and from 51 to 100 μm) per lung section. For each artery, the medial wall thickness was expressed as follows: percent wall thickness = [(medial thickness × 2)/external diameter] × 100. A lung section was obtained from individual rats for comparison among the four groups (n = 5 each).

Hormonal analysis. The plasma AM level was measured by an immunoradiometric assay using a specific kit (Shionogi) (22). For the assessment of right ventricular function (17, 21), the plasma atrial natriuretic peptide (ANP) level was measured using an enzyme immunoassay kit (ANF Rat EIA kit; Peninsula, CA).

Survival analysis. To evaluate the effects of inhaled AM on survival in MCT rats, 20 rats received repeated inhalation of AM (n = 10) or saline (n = 10) four times a day from the date of the MCT injection until death. Survival was estimated from the date of the MCT injection to the death of the rat or 6 wk after the injection.

Statistical analysis. All data are expressed as means ± SE unless otherwise indicated. Comparisons of parameters among three groups were made by one-way ANOVA, followed by Scheffé's multiple-comparison test. Comparisons of the time course of parameters between two groups were made by two-way ANOVA for repeated measures, followed by Scheffé's multiple-comparison test. Survival curves according to the presence or absence of AM inhalation were derived using the Kaplan-Meier method and compared using a log-rank test. A P value <0.05 was considered statistically significant.

RESULTS

Acute effect of single inhalation of AM. Acute hemodynamic studies were carried out at 3 wk after the MCT injection. AM inhalation slightly increased the circulating level of human AM (from 0 to 3.6 ± 1.0 fmol/ml, $P < 0.05$). A 30-min inhalation of AM slightly but significantly decreased the mean pulmonary arterial pressure in MCT rats (from 32 ± 2 to 29 ± 2 mmHg, $P < 0.05$; Fig. 1) without a significant decrease in mean arterial pressure (from 113 ± 5 to 111 ± 4 mmHg, P = not signficant). AM inhalation markedly increased cardiac output by 42% (from 405 ± 22 to 575 ± 34 ml·min^{-1}·kg^{-1}, $P < 0.05$) at the end of inhalation. Thus AM resulted in a 36% decrease in total pulmonary resistance (from 0.081 ± 0.006 to 0.052 ± 0.004 mmHg·ml^{-1}·min^{-1}·kg^{-1}, $P < 0.05$). The ratio of total pulmonary resistance to systemic vascular resistance was significantly decreased at the end of inhalation (from 0.29 ± 0.01 to 0.26 ± 0.01, $P <$ 0.05). Interestingly, these hemodynamic effects of AM lasted at least 60 min after the end of inhalation. Inhalation of saline did not alter any hemodynamic or hormonal parameter.

Chronic effect of repeated inhalation of AM. The physiological profiles of the four experimental groups are summarized in Table 1. Body weight was significantly lower in both MCT groups than in sham rats.

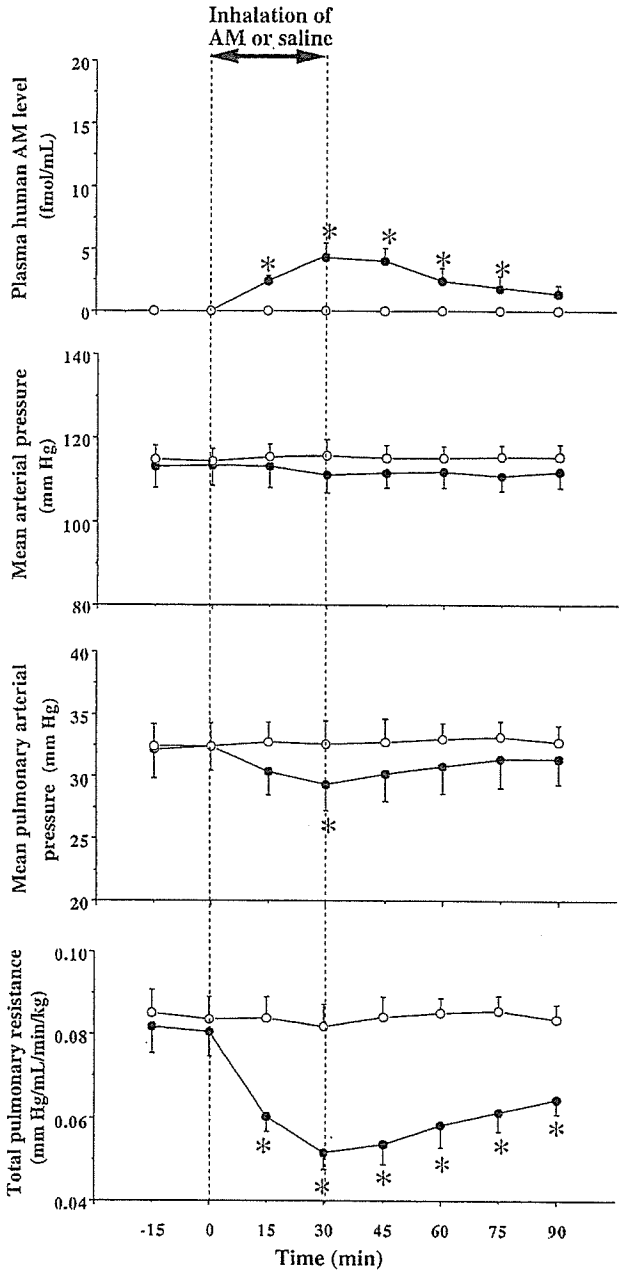

Fig. 1. Acute hemodynamic and hormonal responses to inhaled adrenomedullin (AM; ●) or saline (○) in monocrotaline (MCT)-treated rats (MCT rats). Data are means ± SE. *$P < 0.05$ vs. *time 0*.

Right ventricular weight was significantly lower in MCT rats receiving repeated inhalation of AM than in those given aerosolized saline. There was no significant difference in left ventricular weight among the four groups.

Three weeks after the MCT injection, pulmonary hypertension developed compared with findings in sham rats, but the rise in mean pulmonary arterial pressure was markedly attenuated in MCT rats treated with repeated inhalation of AM (by 37%) compared with that in MCT rats given aerosolized saline (22 ± 2 vs. 35 ± 1 mmHg, $P < 0.05$; Fig. 2). Cardiac output was significantly higher in MCT rats treated with AM (by 30%) compared with that in MCT rats given saline (444 ± 18 vs. 342 ± 18 ml·min^{-1}·kg^{-1}, $P < 0.05$). Therefore, total pulmonary resistance was markedly lower in MCT rats treated with AM (by 54%) compared with that in MCT rats given saline (0.048 ± 0.004 vs. 0.104 ± 0.006 mmHg·ml^{-1}·min^{-1}·kg^{-1}, $P < 0.05$). Similarly, the increase in right ventricular systolic pressure was significantly attenuated by AM inhalation (Table 1). In contrast, neither mean arterial pressure nor heart rate differed among the four groups. The ratio of total pulmonary resistance to systemic vascular resistance was markedly lower in MCT rats treated with aerosolized AM (by 44%) compared with that in MCT rats given aerosolized saline (0.19 ± 0.01 vs. 0.34 ± 0.01, $P < 0.05$). Inhalation of AM did not significantly alter any hemodynamic parameters in sham rats.

Representative photomicrographs of pulmonary arteries showed that hypertrophy of the pulmonary vessel wall was inhibited in MCT rats treated with AM compared with that in MCT rats given saline (Fig. 3). Quantitative analysis of peripheral pulmonary arteries demonstrated that the percent wall thickness of pulmonary arteries was significantly lower in MCT rats treated with aerosolized AM than in those given aerosolized saline (20 ± 1% vs. 28 ± 1% in vasculature with an external diameter of 25–50 μm and 21 ± 1% vs. 27 ± 1% in vasculature with an external diameter of 51–100 μm, both $P < 0.05$; Fig. 3). Inhalation of AM did not significantly alter vascular morphology in sham rats.

Effect of AM inhalation on long-term prognosis in MCT rats. Kaplan-Meier survival curves demonstrated that MCT rats treated with aerosolized AM had a significantly higher survival rate than those given saline (70% vs. 10% in 6-wk survival, log-rank test, $P < 0.01$; Fig. 4). No definite adverse effects were detected after repeated inhalation of AM.

Effect of AM inhalation on developed pulmonary hypertension. AM or saline was inhaled by rats that had developed pulmonary hypertension 3 wk after the MCT injection. Mean pulmonary arterial pressure was significantly lower in MCT rats treated with AM (by 14%) compared with that in rats given saline (32 ± 1 vs. 37 ± 1 mmHg, $P < 0.05$). Cardiac output was also higher in MCT rats treated with AM (by 15%) compared with that in rats given saline (360 ± 11 vs. 313 ± 14 ml·min^{-1}·kg^{-1}, $P < 0.05$). Therefore, total pulmonary resistance was significantly lower in MCT rats treated with AM (by 24%) compared with that in rats given saline (0.091 ± 0.005 vs. 0.119 ± 0.008 mmHg·ml^{-1}·min^{-1}·kg^{-1}, $P < 0.05$).

DISCUSSION

In the present study, we demonstrated that *1*) a single inhalation of AM using an ultrasonic nebulizer induced relatively long-lasting pulmonary vasodilation without systemic hypotension, *2*) repeated inhalation

Table 1. *Physiological profiles of the four experimental groups*

	Sham		MCT	
	Sham-Saline	Sham-AM	MCT-Saline	MCT-AM
n	8	8	8	8
Body weight, g	150 ± 3	154 ± 3	132 ± 2*	146 ± 4†
RV/body wt, g/kg	0.59 ± 0.02	0.58 ± 0.01	0.92 ± 0.06*	0.66 ± 0.02†
LV/body wt, g/kg	2.32 ± 0.04	2.27 ± 0.05	2.48 ± 0.05	2.33 ± 0.05
Heart rate, beats/min	409 ± 15	428 ± 20	424 ± 15	413 ± 14
Mean arterial pressure, mmHg	120 ± 3	117 ± 3	104 ± 3*	115 ± 3†
RV systolic pressure, mmHg	35 ± 1	34 ± 1	67 ± 2*	45 ± 3*†
Right atrial pressure, mmHg	2 ± 1	2 ± 1	7 ± 1*	2 ± 1†
Plasma ANP level, pg/ml	275 ± 40	238 ± 29	694 ± 61*	346 ± 44†

Values are means ± SE; *n*, number of rats. Sham-saline, sham rats given aerosolized saline; sham-AM, sham rats given aerosolized AM; MCT-saline, rats treated with monocrostaline (MCT) and given aerosolized saline; MCT-AM, rats treated with MCT and given aerosolized AM; RV, right ventricular LV, left ventricular; ANP, atrial natriuretic peptide. *$P < 0.05$ vs. sham-saline; †$P < 0.05$ vs. MCT-saline.

of AM ameliorated MCT-induced pulmonary hypertension and attenuated the development of pulmonary vascular remodeling, and *3*) inhalation of AM improved survival in MCT rats without definite adverse effects.

PPH is a rare but life-threatening disease characterized by progressive pulmonary hypertension, ultimately producing right ventricular failure and death (25). Although intravenous administration of prostacyclin has become recognized as a therapeutic breakthrough (1, 6, 16, 26), some patients with PPH are refractory to this treatment. Thus a new therapeutic strategy for the treatment of PPH is desirable.

AM is one of the most potent endogenous vasodilators in the pulmonary vascular bed (5, 13, 14, 22). The vasodilating effect is mediated by a cAMP-dependent and/or nitric oxide-dependent mechanism (10, 20). Recently, we (19) have shown that intravenous administration of AM markedly decreases pulmonary vascular resistance in patients with PPH. Nevertheless, systemically administered AM decreases systemic arterial pressure, which may be harmful in treating patients with PPH. In the present study, inhalation of AM markedly decreased total pulmonary resistance, whereas it did not significantly decrease mean arterial pressure. The ratio of total pulmonary resistance to systemic vascular resistance was significantly reduced by AM inhalation. These results suggest that this novel route of AM administration causes relatively selective pulmonary vasodilation. Expectedly, inhalation of AM markedly increased the cardiac index in MCT rats, consistent with our previous results from intravenous delivery (18). Considering the strong vasodilator activity of AM in the pulmonary vasculature, the significant decrease in cardiac afterload may be responsible for the increased cardiac index with AM. Interestingly, the hemodynamic effects of AM lasted at least 60 min after a single inhalation of AM. Although a single inhalation of AM delivered 0.5 μg AM into the lungs in each rat, it induced only a slight increase in the plasma AM level (3.6 ± 1.0 fmol/ml). These results raise the possibility that inhaled AM is retained in lung tissue for a while and acts transepithelially on the pulmonary vasculature. Thus inhalation of AM may cause potent, long-lasting pulmonary vasodilator activity in MCT rats.

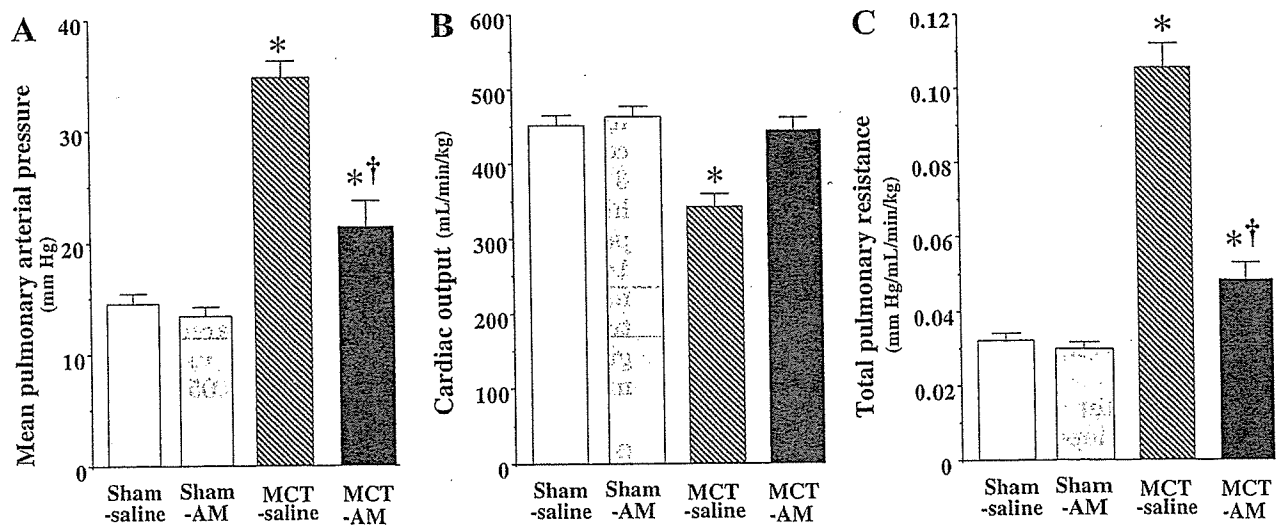

Fig. 2. Chronic effects of AM inhalation on mean pulmonary arterial pressure (*A*), cardiac output (*B*), and total pulmonary resistance (*C*). Sham-saline, sham rats given aerosolized AM; MCT-saline, MCT rats given aerosolized saline; sham-AM, sham rats given aerosolized AM; MCT-AM, MCT rats given aerosolized AM. Data are means ± SE. *$P < 0.05$ vs. sham-saline; †$P < 0.05$ vs. MCT-saline rats.

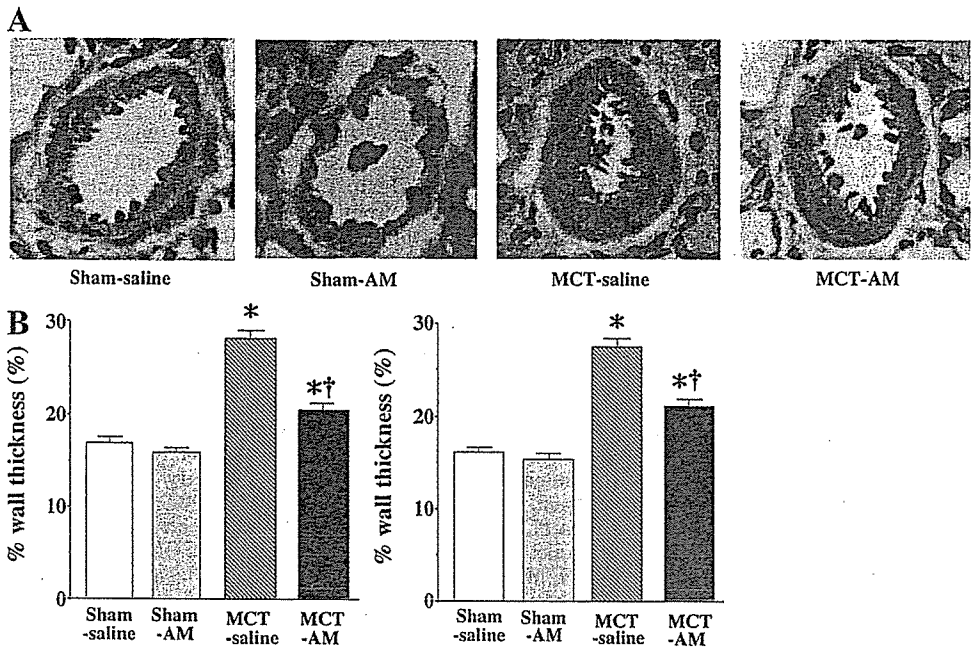

Fig. 3. *A*: representative photomicrographs of peripheral pulmonary arteries in the four groups. AM inhalation markedly inhibited hypertrophy of the vessel wall in MCT rats. Magnification, ×400. *B*: quantitative analyses of peripheral pulmonary arteries with an external diameter of 25–50 μm (*left*) or 51–100 μm (*right*). The percent wall thickness was calculated as [(medial thickness × 2)/external diameter] × 100. Abbreviations are as in Table 1 and Fig. 2. Data are means ± SE. *$P <$ 0.05 vs. sham-saline rats; †$P < 0.05$ vs. MCT-saline rats.

The present study also demonstrated that repeated inhalation of AM four times a day for 3 wk markedly decreased mean pulmonary arterial pressure and total pulmonary resistance in MCT rats without systemic hypotension. The potent, long-lasting pulmonary vasodilator effect of inhaled AM may contribute to the strong inhibition of the development of pulmonary hypertension. In addition, considering intermittent delivery of AM to the lungs, the chronic effects of inhaled AM appear to go beyond acute pulmonary vasodilation. In the present study, inhalation of AM inhibited an increase in the medial wall thickness of peripheral pulmonary arteries of MCT rats. Earlier studies (8, 12) have shown that AM inhibits the migration and proliferation of vascular smooth muscle cells. Given the known potent vasoprotective effects of AM, such as vasodilation and inhibition of smooth muscle cell migration and proliferation, it is interesting to speculate that AM trapped in the bronchial epithelium or alveoli leaks to the pulmonary arteries to maintain pulmonary vascular integrity in MCT rats. Inhalation of AM also decreased plasma ANP, a potential marker for right ventricular dysfunction (17, 21). It is possible that the decreased pulmonary vascular resistance by AM may ameliorate increased wall stress in the right ventricle and improve right ventricular dysfunction in MCT rats.

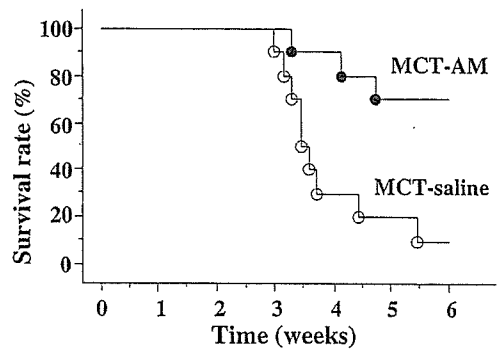

Fig. 4. Kaplan-Meier survival curves showing that MCT rats treated with aerosolized AM had a significantly higher survival rate than those given saline inhalation (log-rank test, $P < 0.01$).

Importantly, Kaplan-Meier analysis demonstrated that the 6-wk survival rate for MCT rats treated with aerosolized AM was significantly high (70%) compared with those given saline (10%). Thus treatment with aerosolized AM may be an alternative approach for severe pulmonary hypertension that is refractory to conventional therapy.

In the pulmonary circulation, the AM receptor acts not only as a functional receptor but also as a clearance receptor, the expression of which is stimulated by basal AM itself (3). Thus exogenously administered AM may have differing effects depending on the basal levels of AM.

Champion et al. (2) showed that intratracheal gene transfer of prepro-calcitonin gene-related peptide (CGRP) to the lung attenuates chronic hypoxia-induced pulmonary hypertension in mice. The gene for AM belongs to the CGRP family, and the receptors for CGRP and AM bind both peptides (15). In addition, the AM receptor is expressed at high levels in the pulmonary vascular endothelium, and there is an interaction of CGRP and AM with the receptor in the pulmonary endothelium (4). Thus it is not surprising that AM attenuates pulmonary hypertension in a similar manner as CGRP. In fact, we (31) have previously reported a beneficial effect of AM in a rat model of pulmonary hypertension. In our previous study, however, AM was administered subcutaneously. In contrast, in the present study, AM was inhaled to ameriolate pulmonary hypertension, which may have a pharmacological

and clinical implication of the treatment for this disorder.

In conclusion, repeated inhalation of AM inhibited MCT-induced pulmonary hypertension without systemic hypotension and thereby improved survival in MCT rats. Thus long-term treatment with aerosolized AM may be a new therapeutic strategy for the treatment of pulmonary hypertension.

We thank Yumi Takara for technical assistance.

DISCLOSURES

This work was supported by grants from the Japan Cardiovascular Research Foundation, Kanae Foundation for Life and Sociomedical Science, Research on Health Sciences Focusing on Drug Innovation, Research Grant for Cardiovascular Disease 12C-2 from the Ministry of Health, Labour and Welfare, and the Promotion of Fundamental Studies in Health Science of the Organization for Pharmaceutical Safety and Research of Japan.

REFERENCES

1. **Barst RJ, Rubin LJ, Long WA, McGoon MD, Rich S, Badesch DB, Groves BM, Tapson VF, Bourge RC, Brundage BH, Koerner SK, Langleben D, Keller CA, Murali S, Uretsky BF, Clayton LM, Jobsis MM, Blackburn SD, Shortino D, and Crow JW.** A comparison of continuous intravenous epoprostenol (prostacyclin) with conventional therapy for primary pulmonary hypertension. *N Engl J Med* 334: 296–301, 1996.
2. **Champion HC, Bivalacqua TJ, Toyoda K, Heistad DD, Hyman AL, and Kadowitz PJ.** In vivo gene transfer of prepro-calcitonin gene-related peptide to the lung attenuates chronic hypoxia-induced pulmonary hypertension in the mouse. *Circulation* 101: 923–930, 2000.
3. **Dschietzig T, Azad HA, Asswad L, Bohme C, Bartsch C, Baumann G, and Stangl K.** The adrenomedullin receptor acts as clearance receptor in pulmonary circulation. *Biochem Biophys Res Commun* 294: 315–318, 2002.
4. **Han ZQ, Coppock HA, Smith DM, Van Noorden S, Makgoba MW, Nicholl CG, and Legon S.** The interaction of CGRP and adrenomedullin with a receptor expressed in the rat pulmonary vascular endothelium. *J Mol Endocrinol* 18: 267–272, 1997.
5. **Heaton J, Lin B, Chang JK, Steinberg S, Hyman A, and Lippton H.** Pulmonary vasodilation to adrenomedullin: a novel peptide in humans. *Am J Physiol Heart Circ Physiol* 268: H2211–H2215, 1995.
6. **Higenbottam TW, Wheeldon D, Wells FC, and Wallwork J.** Long-term treatment of primary pulmonary hypertension with continuous intravenous epoprostenol (prostacyclin). *Lancet* 1: 1046–1047, 1984.
7. **Hoeper MM, Schwarze M, Ehlerding S, Adler-Schuermeyer A, Spiekerkoetter E, Niedermeyer J, Hamm M, and Fabel H.** Long-term treatment of primary pulmonary hypertension with aerosolized iloprost, a prostacyclin analogue. *N Engl J Med* 342: 1866–1870, 2000.
8. **Horio T, Kohno M, Kano H, Ikeda M, Yasunari K, Yokokawa K, Minami M, and Takeda T.** Adrenomedullin as a novel antimigration factor of vascular smooth muscle cells. *Circ Res* 77: 660–664, 1995.
9. **Ichiki Y, Kitamura K, Kangawa K, Kawamoto M, Matsuo H, and Eto T.** Distribution and characterization of immunoreactive adrenomedullin in human tissue and plasma. *FEBS Lett* 338: 6–10, 1994.
10. **Ishizaka Y, Ishizaka Y, Tanaka M, Kitamura K, Kangawa K, Minamino N, Matsuo H, and Eto T.** Adrenomedullin stimulates cyclic AMP formation in rat vascular smooth muscle cells. *Biochem Biophys Res Commun* 200: 642–646, 1994.
11. **Kakishita M, Nishikimi T, Okano Y, Satoh T, Kyotani S, Nagaya N, Fukushima K, Nakanishi N, Takishita S, Miyata A, Kangawa K, Matsuo H, and Kunieda T.** Increased plasma levels of adrenomedullin in patients with pulmonary hypertension. *Clin Sci (Lond)* 96: 33–39, 1999.
12. **Kano H, Kohno M, Yasunari K, Yokokawa K, Horio T, Ikeda M, Minami M, Hanehira T, Takeda T, and Yoshikawa J.** Adrenomedullin as a novel antiproliferative factor of vascular smooth muscle cells. *J Hypertens* 14: 209–213, 1996.
13. **Kitamura K, Kangawa K, Kawamoto M, Ichiki Y, Nakamura S, Matsuo H, and Eto T.** Adrenomedullin: a novel hypotensive peptide isolated from human pheochromocytoma. *Biochem Biophys Res Commun* 192: 553–560, 1993.
14. **Lippton H, Chang JK, Hao Q, Summer W, and Hyman AL.** Adrenomedullin dilates the pulmonary vascular bed in vivo. *J Appl Physiol* 76: 2154–2156, 1994.
15. **McLatchie LM, Fraser NJ, Main MJ, Wise A, Brown J, Thompson N, Solari R, Lee MG, and Foord SM.** RAMPs regulate the transport and ligand specificity of the calcitonin-receptor-like receptor. *Nature* 393: 333–339, 1998.
16. **McLaughlin VV, Genthner DE, Panella MM, and Rich S.** Reduction in pulmonary vascular resistance with long-term epoprostenol (prostacyclin) therapy in primary pulmonary hypertension. *N Engl J Med* 338: 273–277, 1998.
17. **Nagaya N, Nishikimi T, Uematsu M, Satoh T, Kyotani S, Sakamaki F, Kakishita M, Fukushima K, Okano Y, Nakanishi N, Miyatake K, and Kangawa K.** Plasma brain natriuretic peptide as a prognostic indicator in patients with primary pulmonary hypertension. *Circulation* 102: 865–870, 2000.
18. **Nagaya N, Nishikimi T, Uematsu M, Satoh T, Oya H, Kyotani S, Sakamaki F, Ueno K, Nakanishi N, Miyatake K, and Kangawa K.** Hemodynamic and hormonal effects of adrenomedullin in patients with pulmonary hypertension. *Heart* 84: 653–658, 2000.
19. **Nagaya N, Satoh T, Nishikimi T, Uematsu M, Furuichi S, Sakamaki F, Oya H, Kyotani S, Nakanishi N, Goto Y, Masuda Y, Miyatake K, and Kangawa K.** Hemodynamic, renal and hormonal effects of adrenomedullin infusion in patients with congestive heart failure. *Circulation* 101: 498–503, 2000.
20. **Nakamura M, Yoshida H, Makita S, Arakawa N, Niinuma H, and Hiramori K.** Potent and long-lasting vasodilatory effects of adrenomedullin in humans: comparisons between normal subjects and patients with chronic heart failure. *Circulation* 95: 1214–1221, 1997.
21. **Nootens M, Kaufmann E, Rector T, Toher C, Judd D, Francis GS, and Rich S.** Neurohormonal activation in patients with right ventricular failure from pulmonary hypertension: relation to hemodynamic variables and endothelin levels. *J Am Coll Cardiol* 26: 1581–1585, 1995.
22. **Nossaman BD, Feng CJ, Kaye AD, DeWitt B, Coy DH, Murphy WA, and Kadowitz PJ.** Pulmonary vasodilator responses to adrenomedullin are reduced by NOS inhibitors in rats but not in cats. *Am J Physiol Lung Cell Mol Physiol* 270: L782–L789, 1996.
23. **Ono S and Voelkel NF.** PAF antagonists inhibit monocrotaline-induced lung injury and pulmonary hypertension. *J Appl Physiol* 71: 2483–2492, 1991.
24. **Owji AA, Smith DM, Coppock HA, Morgan DG, Bhogal R, Ghatei MA, and Bloom SR.** An abundant and specific binding site for the novel vasodilator adrenomedullin in the rat. *Endocrinology* 136: 2127–2134, 1995.
25. **Rich S, Dantzker DR, Ayres SM, Bergofsky EH, Brundage BH, Detre KM, Fishman AP, Goldring RM, Groves BM, Koerner SK, Levy PC, Reid LM, Vreim CE, and Williams GW.** Primary pumonary hypertension: a national prospective study. *Ann Intern Med* 107: 216–223, 1987.
26. **Rubin LJ, Mendoza J, Hood M, McGoon M, Barst R, Williams WB, Diehl JH, Crow J, and Long W.** Treatment of primary pulmonary hypertension with continuous intravenous prostacyclin (epoprostenol): results of a randomized trial. *Ann Intern Med* 112: 485–491, 1990.
27. **Sakata J, Shimokubo T, Kitamura K, Nishizono M, Iehiki Y, Kangawa K, Matsuo H, and Eto T.** Distribution and characterization of immunoreactive rat adrenomedullin in tissue and plasma. *FEBS Lett* 352: 105–108, 1994.
28. **Walmrath D, Schneider T, Pilch J, Grimminger F, and Seeger W.** Aerosolized prostacyclin reduces pulmonary artery

pressure and improves gas exchange in the adult respiratory distress syndrome (ARDS). *Lancet* 342: 961–962, 1993.

29. **Wensel R, Opitz CF, Ewert R, Bruch L, and Kleber FX.** Effects of iloprost inhalation on exercise capacity and ventilatory efficiency in patients with primary pulmonary hypertension. *Circulation* 101: 2388–2392, 2000.
30. **Yoshibayashi M, Kamiya T, Kitamura K, Saito Y, Kangawa K, Nishikimi T, Matsuoka H, Eto T, and Matsuo H.** Plasma levels of adrenomedullin in primary and secondary pulmonary hypertension in patients < 20 years of age. *Am J Cardiol* 79: 1556–1558, 1997.
31. **Yoshihara F, Nishikimi T, Horio T, Yutani C, Takishita S, Matsuo H, Ohe T, and Kangawa K.** Chronic infusion of adrenomedullin reduces pulmonary hypertension and lessens right ventricular hypertrophy in rats administered monocrotaline. *Eur J Pharmacol* 355: 33–39, 1998.

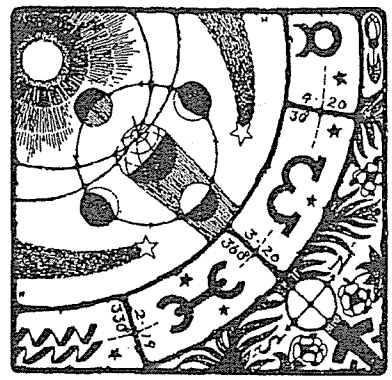

Applications of stroboscopic x-ray generators to high-speed radiographies including biomedical applications

Haruo Obara[a], Masayuki Zuguchi[a], Eiichi Sato[b], Etsuro Tanaka[c], Hidezo Mori[d], Tatsumi Usuki[e], Koetsu Sato[e], Hidenori Ojima[f] and Kazuyoshi Takayama[f]

[a] Department of Radiological Technology, College of Medical Science, Tohoku University, 1-1 Seiryocho, Sendai 980-0872, Japan
[b] Department of Physics, Iwate Medical University, 3-16-1 Honchodori, Morioka 020-0015, Japan
[c] Department of Physiology, School of Medicine, Tokai University, Boseidai, Isehara 259-1193, Japan
[d] Department of Cardiac Physiology, National Cardiovascular Center Research Institute, 5-7-1 Fujishirodai, Suita, Osaka 565-8565 Japan
[e] Toreck Inc., 5-6-20 Tsunashima Higashi, Yokohama 223-0052, Japan
[f] Shock Wave Research Center, Institute of Fluid Science, Tohoku University, 2-1-1 Katahira, Sendai 980-8577, Japan

ABSTRACT

The constructions and major characteristics of recent stroboscopic x-ray generators and their applications to high-speed radiographies including biomedical applications are described. The generators are as follows: (a) a 100 kV generator having a fixed-anode radiation tube, (b) a 120 kV medical generator with a rotating-anode tube, and (c) a 300 keV generator utilizing a fixed-anode tube. The type (a) and (b) generators employ large-capacity condensers of about 500 nF, and the electric charges in the condensers are discharged repetitively to each tube by controlling the grid voltage. The x-ray duration can be controlled from 0.01 to 1.0 ms, and the intensity increases with increases in the charging voltage, the duration, and the filament voltage. When the external triggering system is employed, the maximum repetition rate has a value of 50 kHz. Next, the type (c) generator has a high-voltage transformer and produces short x-ray pulses with widths of about 300 ns, and the maximum rate is about 1 kHz. The high-speed radiography was performed using a film-less computed radiography (CR) system, and stop-motion images of objects were obtained.

Keywords: Stroboscopic x-ray, Repetitive x-ray, Computed radiography, Medical radiography

1. INTRODUCTION

With recent advances in high-voltage pulse technology, various flash x-ray generators[1] have been developed corresponding to the radiographic objectives, and flash x-ray generators with photon energies of less than 150 keV have been developed in order to perform soft radiographies including biomedical applications.[2-8] Because there is not much ultra high-speed motions in biomedical radiography, the stroboscopic x-ray generators[9-11] are quite useful for obtaining stop-motion images.

The stroboscopic x-ray generators produce repetitive x-rays and perform multiple-shot and cine radiographies. For the first time, we have developed a compact condenser-discharge stroboscopic x-ray generator with a maximum condenser charging voltage of 100 kV and repetition rate of 32 kHz, respectively. Using this generator, the x-ray duration can be controlled from 0.01 to 1.0 ms, and the sufficient x-ray intensity for a computed radiography (CR) system[12] has been obtained. In the medical field, there are various condenser-discharge x-ray generators, and these generators can be reconstructed as stroboscopic x-ray generators by equipping a new grid control unit. Furthermore, the maximum photon energy can be increased up to about 150 kV, because the anode and cathode of the x-ray tube are applied to positive and negative high voltages, respectively.

Under the pulse operation, the high-voltage durability of the x-ray tube substantially increases, and high photon energy x-rays can be easily produced even when a fixed-anode tube with a maximum voltage of 100 kV is employed.
In this paper, we report on stroboscopic x-ray generators recently developed by the authors and radiographies including biomedical applications achieved with the CR system.

2. STROBOSCOPIC X-RAY GENERATORS

2.1. 100 kV Generator

The 100 kV generator (Figure 1) consists of the following major components: a main controller, a condenser unit having a Cockcroft circuit, and an x-ray tube unit in conjunction with a grid controller. The main condenser of about 500 nF in the unit is charged up to 100 kV by the circuit, and the electric charges in the condenser are discharged to the triode by the grid controller. Although the tube voltage decreased during the discharging for generating x-rays, the maximum value was equivalent to the initial charging voltage of the main condenser.

2.2. 120 kV Medical Generator

The 120 kV generator (Figure 2) employs a condenser-discharge medical x-ray generator in conjunction with a new grid-control unit and consists of the following major components: a high-voltage control unit, a condenser unit having a Cockcroft circuit, a grid-control unit, a high-voltage grid-control unit, and a rotating-anode x-ray tube unit. The main condenser of about 500 nF in the unit is charged up to 120 kV by the circuit, and the electric charges in the condenser are discharged to the triode by the grid-control unit in conjunction with a high-voltage grid-control unit. This unit is employed in order to insulate the negative high-voltage grid and cathode electrodes from the high-speed grid control unit with almost the ground potential. In this generator, the anode and cathode electrodes are applied to high-voltages with maximum values of +60 kV and -60 kV, respectively. Although the tube voltage decreased during the discharging for generating x-rays, the maximum value was equal to the initial charging voltage of the main condenser.

2.3. 300 kV Generator

The 300 kV generator (Figure 3) is developed in order to increase the maximum photon energy of the pulse x-rays because the high-voltage durability of the x-ray tube substantially increases under the pulse operation. The setup is composed of the following essential components: a thyratron pulse generator, a high-voltage transformer having a ferrite core with a maximum output voltage of 300 kV, a sequence controller, a DC power supply for the hot cathode (filament), and an x-ray tube. The main condenser of 50 nF in the pulse generator is charged up to 15 kV, and the electric charges in the condenser are discharged repetitively to the primary coil of the transformer. Because the high-voltage pulses from the secondary coil are then applied to the x-ray tube, repetitive harder x-rays are produced. The energy-storage condenser of 2.0 μF is employed to increase the repetition rate of x-rays. Both the transformer and the x-ray tube are set in the oil tank having an x-ray window, and the pulse x-rays are produced from the window.

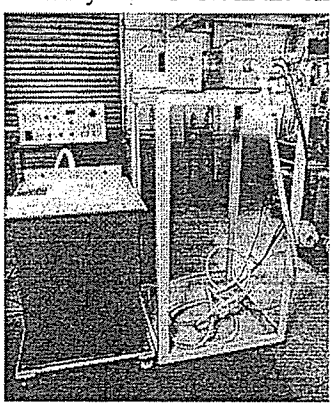

Figure 1. General view of The 100 kV stroboscopic x-ray generator.

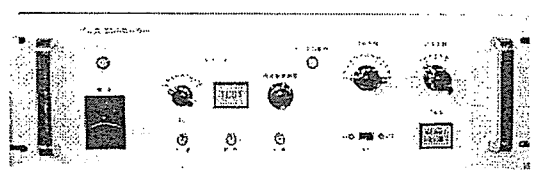

Figure 2. Control panel of the grid control unit in the 120 kV generator.

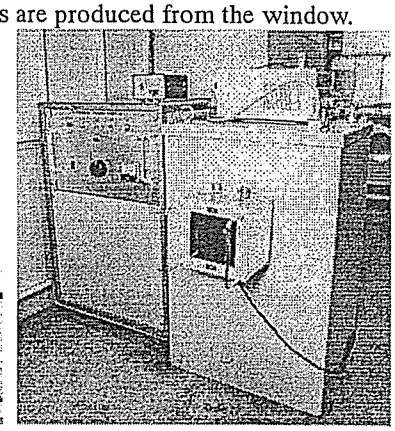

Figure 3. 300 kV stroboscopic x-ray generator.

3. RADIOGRAPHIC CHARACTERISTICS

3.1. Characteristics of 100 kV Generator

The x-ray output was measured by a combination of a plastic scintillator and a photomultiplier. In order to decrease the electric noise, the fluorescent outputs from the scintillator were leaded to a photomultiplier through a plastic fiber, and the output voltages from the photomultiplier were recorded by a digital storage scope. The time constant of the measuring circuit of the photomultiplier had a value of 500 ns in order to measure the short pulse width of 10 μs with accuracy. Figure 4 shows the x-ray output according to changes in the driving pulse width of x-rays at a constant

charging voltage of 70 kV. We observed many peaks due to the time constant of the circuit, and the pulse width of x-rays corresponded well to the driving width. At a constant driving pulse width, the pulse height increased when the charging voltage was increased. The pulse width of the x-rays ranged from 0.01 to 1.0 ms, and the maximum shot number had a value of 32. When the external triggering system is employed, the maximum repetition rate had a value of 50 kHz.

3.2. Characteristics of 120 kV Generator

The repetitive x-ray outputs from the medical generator with a charging voltage of 90 kV is shown in Figure 5. This generator produced comparatively stable repetitive x-rays and had almost the same radiographic characteristics as in the 100 kV generator. The pulse width of the x-rays could be controlled up to 1.0 ms, and the maximum shot number was 32.

3.3. Characteristics of 300 kV Generator

Because this generator produces high-photon-energy x-rays, the x-ray transmissivity is an important factor. Figure 6 shows results of the transmission test using aluminum filters. Although the height decreased according to increases in the thickness of the filter, the x-rays easily transmitted even when a 25 mm filter was employed. Using this generator, the width of the first x-ray pulse and the maximum rate had values of about 300 ns and 1 kHz, respectively.

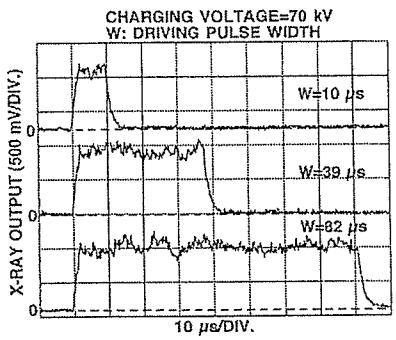

Figure 4. X-ray outputs from the 100 kV generator with corresponding changes of the driving pulse width at a constant charging voltage of 70 kV.

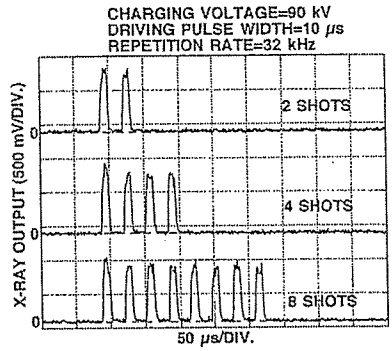

Figure 5. Repetitive x-ray outputs from the medical generator with a charging voltage of 90 kV.

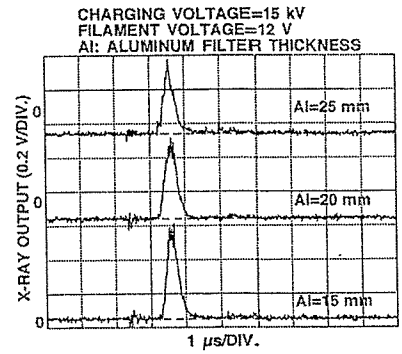

Figure 6. X-ray output from the 300 kV generator according to changes in the thickness of the aluminum filter.

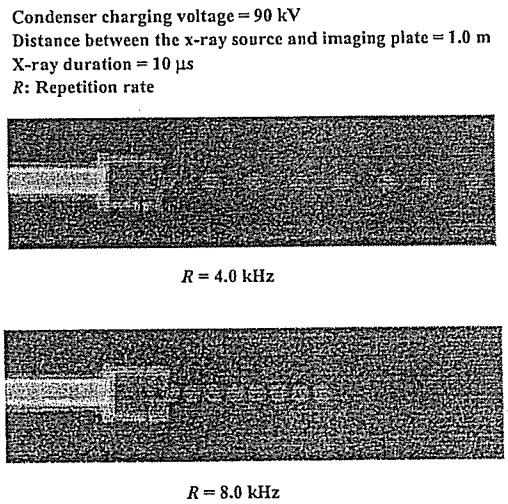

Figure 7. Multiple-shot radiogram of a plastic bullet.

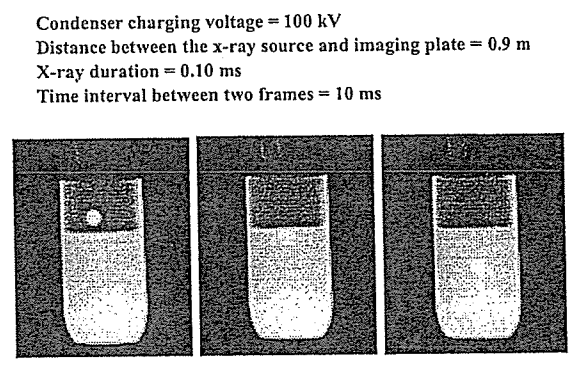

Figure 8. Delayed radiograms of the iron ball.

Condenser charging voltage = 90 kV
Distance between the x-ray source and imaging plate = 0.7 m
X-ray duration = 0.22 ms
D: Delay time after explosion

D = 0.60 ms *D* = 0.80 ms

Figure 9. Delayed radiography of the cavitation bubble cloud induced by underwater shock wave focusing in living frog.

Condenser charging voltage = 70 kV
Distance between the x-ray source and imaging plate = 1.0 m
X-ray duration = 1.0 ms

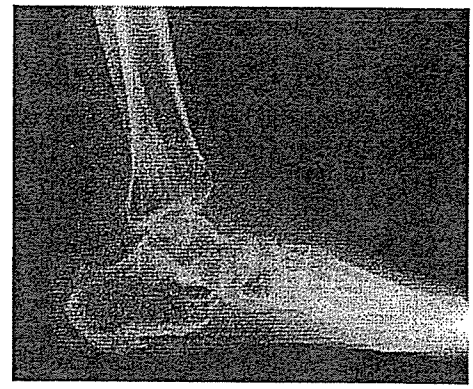

Figure 10. Radiogram of a leg.

Condenser charging voltage = 120 kV
Distance between the x-ray source and imaging plate = 1.8 m
X-ray duration = 1.0 ms

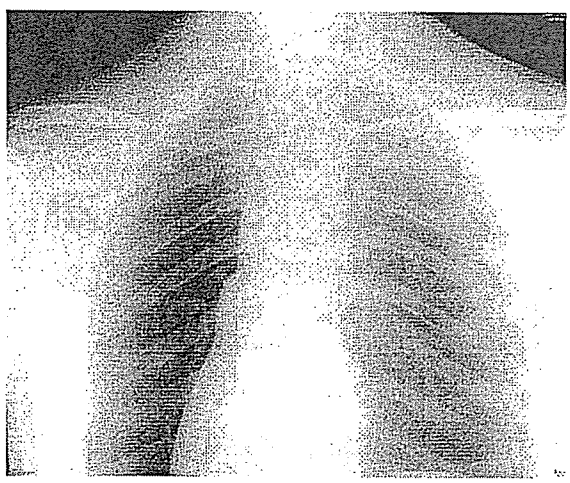

Figure 11. Chest radiogram.

Condenser charging voltage = 70 kV
Distance between the x-ray source and imaging plate = 1.8 m
X-ray duration = 1.0 ms
T: PMMA thickness

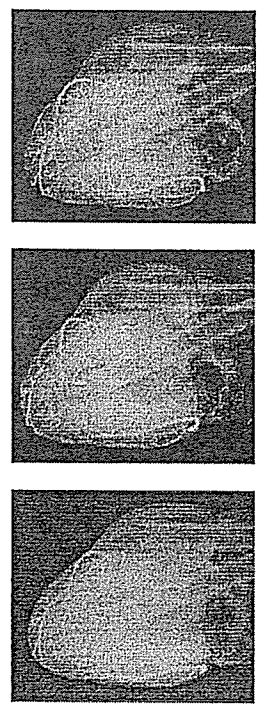

T = 0 mm

T = 10 mm

T = 30 mm

Figure 12. Radiograms of a heart of a dog according to changes in the thickness of inserted PMMA plate.

4. RADIOGRAPHY

The radiography was performed by the CR system. The radiograms obtained by using the 100 kV generator are shown in Figures 7~10. Figure 7 shows the multiple-shot radiograms of a plastic bullet at the indicated conditions. Because we employed a short x-ray duration of 10 μs, we obtained almost stop-motion images of a bullet. Next, the delayed

radiography was achieved with one shot of x-rays using a trigger-delay device. The delayed radiograms of the iron ball are shown in Figure 8, and the stop-motion images of a ball are visible. Delayed radiography of the cavitation bubble cloud induced by underwater shock wave focusing in a living frog is shown in Figure 9. In these cases, we could observe the large bubble cloud in front of the abdomen at the side facing the reflector with a delay time of 0.6 ms. However, we hardly observed the bubble in a frog.

Since the 120 kV generator produces higher intensity x-rays as compared with the 100 kV generator, various portions of a human body can be taken (Figures 11~13). A chest radiogram of a human phantom is shown in Figure 11, and we obtained almost the same image to one obtained by the conventional medical x-ray generator.

Figure 12 shows angiograms of a heart extracted from a dog according to changes in the thickness of polymethyl methacrylate (PMMA) that is located in front of the heart. The image contrast of blood vessels decreased with corresponding increases in the thickness, and we observed fine vessels clearly in an enlarged radiogram (Figure 13) without using a PMMA plate.

The multiple-shot radiogram of a falling mail screw is shown in Fig. 14, and the image was achieved with 4 shots of repetitive x-rays and a 300 keV generator. In this radiography, stop-motion images of a screw from an aluminum tube are visible.

Condenser charging voltage = 70 kV
Distance between the x-ray source and imaging plate = 1.8 m
X-ray duration = 1.0 ms
PMMA thickness = 0 mm

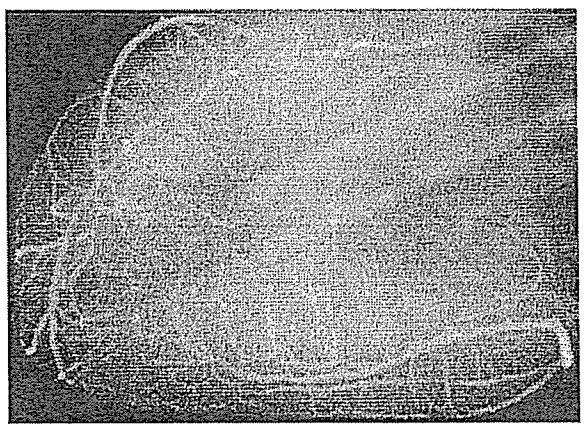

Figure 13. Enlarged radiogram of a heart without using a PMMA plate.

Maximum tube voltage = about 300 kV
Distance between the x-ray source and imaging plate = 0.7 m
Effective x-ray duration = about 300 ns
Repetition rate = 125 Hz

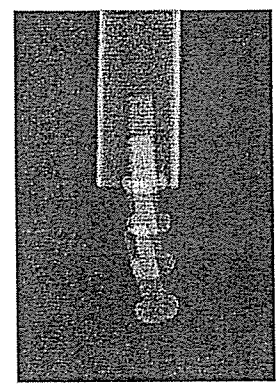

Figure 14. Multiple-shot radiogram of a falling male screw achieved with 4 shots of repetitive x-rays.

5. DISCUSSION

As compared with flash x-ray generators, the stroboscopic x-ray generators produce lower dose rate pulse x-rays with longer durations. However, when the condenser-discharge generators are employed, the repetition rate can be increased up to MHz. On the other hand, although the 300 kV generator produces lower x-ray intensities per pulse, the x-ray qualities are very hard.

In the condenser-discharge generator, the tube voltage and the current are almost constant during the discharge for generating x-rays and have values of V_c and J, respectively, the spectrum distribution of the bremsstrahlung x-rays $S(E)$ is approximated by the following simple equation:

$$S(E) = K_1 J (E_0 - E), \quad (1)$$

where E is the photon energy, E_0 is the maximum photon energy corresponding to V_c, and K_1 is a constant.

The high-photon-energy stroboscopic x-ray generator with a maximum photon energy of about 300 keV has been designed in order to increase the photon energy and to decrease the pulse width of x-rays, and we have succeeded in producing almost single pulse x-rays with a width of about 300 ns.

Because the x-ray output displayed almost the single pulse, the tube voltage $V(t)$ is approximated by:

$$V(t) \cong V_0 \sin \beta t,$$
$$\beta = \{(4L / C_s) - R^2\}^{0.5} / 2L = 2\pi / T, \qquad (0 \le t \le T/2). \tag{2}$$

Here, V_0 is the maximum voltage that is almost equal to the secondary peak voltage from the transformer, C_s is the stray capacity, T is the oscillation period, and R and L are the resistance and the inductance in the secondary circuit, respectively. Next, the tube current $J'(t)$ varies according to changes in the tube voltage and the cathode temperature, and the current increases with corresponding increases in both the tube voltage and temperature. Thus the bremsstrahlung x-ray spectra $S'(E)$ by one shot is approximated by:

$$S'(E) \cong K_2 \int_0^{T/2} J'(t) (E'_0 \sin \beta t - E)\, dt, \tag{3}$$

where E'_0 is the maximum photon energy corresponding to V_0 and K_2 is a constant.

Although the duration can be controlled in the condenser-discharge stroboscopic x-ray generators, the duration has a constant in the case where the transformer-driven generator is employed. Using these stroboscopic x-ray generators, because the optimum generator can be selected corresponding to the radiographic objectives, these generators can be applied to perform high-speed radiography for imaging a wide variety of objects.

ACNOWLEDGMENT

This work was supported by Grants from Test of Fostering Potential of Japan Science and Technology Corporation and Ministry of Education, Culture, Sports, and Science and Technology in Japan.

REFERENCES

1. R. Germer, "X-ray flash techniques," *J. Phys. E: Sci. Instrum.*, **12**, pp. 336-350, 1979.

2. E. Sato, S. Kimura, S. Kawasaki, H. Isobe, K. Takahashi, Y. Tamakawa and T. Yanagisawa, "Repetitive flash x-ray generator utilizing a simple diode with a new type of energy-selective function," *Rev. Sci. Instrum.*, **61**, pp. 2343-2348, 1990.

3. A. Shikoda, E. Sato, M. Sagae, T. Oizumi, Y. Tamakawa and T. Yanagisawa, "Repetitive flash x-ray generator having a high-durability diode driven by a two-cable-type line pulser," *Rev. Sci. Instrum.*, **65**, pp. 850-856, 1994.

4. E. Sato, K. Takahashi, M. Sagae, S. Kimura, T. Oizumi, Y. Hayasi, Y. Tamakawa and T. Yanagisawa, "Sub-kilohertz flash x-ray generator utilizing a glass-enclosed cold-cathode triode," *Med. & Biol. Eng. & Comput.*, **32**, pp. 289-294, 1994.

5. K. Takahashi, E. Sato, M. Sagae, T. Oizumi, Y. Tamakawa and T. Yanagisawa, "Fundamental study on a long-duration flash x-ray generator with a surface-discharge triode," *Jpn. J. Appl. Phys.*, **33**, pp. 4146-4151, 1994.

6. E. Sato, M. Sagae, A. Shikoda, K. Takahashi, T. Oizumi, M. Yamamoto, A. Takabe, K. Sakamaki, Y. Hayasi, H. Ojima, K. Takayama and Y. Tamakawa, "High-speed soft x-ray techniques," *SPIE*, **2869**, pp. 937-955, 1996.

7. E. Sato, Y. Hayashi, E. Tanaka, H. Mori, T. Kawai, H. Obara, T. Ichimaru, K. Takayama, H. Ido, T. Usuki, K. Sato and Y. Tamakawa, "Polycapillary radiography using a quasi-x-ray laser generator," *SPIE*, **4508**, pp. 176-187, 2001.

8. E. Sato, Y. Hayasi, E. Tanaka, H. Mori, T. Kawai, T. Usuki, K. Sato, H. Obara, T. Ichimaru, K. Takayama, H. Ido and Y. Tamakawa, "Quasi-monochromatic radiography using a high-intensity quasi-x-ray laser generator," *SPIE*, **4682**, pp. 538-548 2002.

9. E. Sato, M. Sagae, K. Takahashi, A. Shikoda, T. Oizumi, Y. Hayasi, Y. Tamakawa and T. Yanagisawa, "10 kHz microsecond pulsed x-ray generator utilizing a hot-cathode triode with variable durations for biomedical radiography," *Med. & Biol. Eng. & Comput.*, **32**, pp. 295-301, 1994.

10. H. Obara, M. Zuguchi, E. Sato, T. Usuki, K. Sato, H. Ojima, K. Takayama and Y. Tamakawa, "Application of harder stroboscopic x-ray generator to high-speed radiography," *SPIE*, **4183**, pp. 355-364, 2000.

11. E. Sato, Y. Hayasi and Y. Tamakawa, "Recent stroboscopic x-ray generators and their applications to high-speed radiography," *Ann. Rep. Iwate Med. Univ. Lib. Arts and Sci.*, **35**, pp. 1-11, 2000.

12. E. Sato, K. Sato and Y. Tamakawa, "Film-less computed radiography system for high-speed Imaging," *Ann. Rep. Iwate Med. Univ. Lib. Arts and Sci.*, **35**, pp. 13-23, 2000.

EphA4-Mediated Rho Activation via Vsm-RhoGEF Expressed Specifically in Vascular Smooth Muscle Cells

Hisakazu Ogita, Satoshi Kunimoto, Yuji Kamioka, Hirofumi Sawa, Michitaka Masuda, Naoki Mochizuki

Abstract—Rho-kinase, an effector of Rho GTPase, increases the contractility of vascular smooth muscle by phosphorylating myosin light chain (MLC) and by inactivating MLC phosphatase. A wide variety of extracellular stimuli activate RhoA via G protein–coupled receptors. In the present study, we demonstrate a novel cell-cell interaction–mediated Rho activation signaling pathway in vascular smooth muscle cells (VSMCs). Among many receptor tyrosine kinases, the Eph family receptors are unique in that they require cell-cell interaction to engage their ligands, ephrin. We found that a novel VSMC-specific guanine nucleotide exchange factor (GEF) for Rho (Vsm-RhoGEF/KIAA0915) was expressed specifically in VSMCs of several organs including the heart, aorta, liver, kidney, and spleen, as examined by the immunohistochemical analysis using a specific antibody against Vsm-RhoGEF. Based on the association of Vsm-RhoGEF with EphA4 in quiescent cells, we tested whether EphA4 and Vsm-RhoGEF were expressed in the same tissue and further studied the molecular mechanism of Vsm-RhoGEF regulation by EphA4. Immunohistochemical analysis showed that EphA4 and Vsm-RhoGEF expression overlapped in VSMCs. Additionally, tyrosine phosphorylation of Vsm-RhoGEF induced by EphA4 upon ephrin-A1 stimulation enhanced the Vsm-RhoGEF activity for RhoA. The requirement of Vsm-RhoGEF for ephrin-A1–induced assembly of actin stress fibers in VSMCs was shown by the overexpression of a dominant-negative form of VSM-RhoGEF and by the depletion of Vsm-RhoGEF using RNA interference. These results suggested that ephrin-A1–triggered EphA4-Vsm-RhoGEF-RhoA pathway is involved in the cell-cell interaction–mediated RhoA activation that regulates vascular smooth muscle contractility. (***Circ Res*. 2003;93: 23-31.**)

Key Words: smooth muscle cells ■ Rho ■ Eph ■ ephrin ■ contraction

Vascular smooth muscle cell (VSMC) contractility regulates vascular tone to maintain blood circulation. Increased vascular smooth muscle contraction results in spasm and chronic contraction leads to hypertension, both of which contribute to cardiovascular pathology. Vascular contraction is regulated by actin-myosin II coupling in a Ca^{2+}-dependent manner and a Ca^{2+}-independent manner. The Rho GTPases play an important role in the Ca^{2+}-independent vascular contraction, known as Ca^{2+} sensitization.[1]

Myosin II is regulated by phosphorylation and dephosphorylation of the myosin regulatory light chain. The former is controlled by myosin light chain (MLC) kinase regulated by Ca^{2+}/calmodulin, and the latter is regulated by MLC phosphatase (MLCP). Recently, RhoA has been shown to be involved in the inhibition of MLCP via the Rho effector molecule, Rho-kinase. The phosphorylation of MLCP inhibits the phosphatase activity and thereby activates MLC,[2] resulting in contraction of smooth muscle. In addition to MLCP phosphorylation, Rho-kinase directly phosphorylates MLC and increases the contractility of myosin II.[3] These data support that Rho activation is clinically involved in vasospastic angina and unfavorable smooth muscle contraction of atherosclerotic arteries.[4,5]

The Rho GTPase functions as a molecular switch by cycling between a GTP-bound active form and a GDP-bound inactive form. This cycle is regulated by three classes of molecules: guanine nucleotide exchange factors (GEFs), guanine nucleotide dissociation inhibitors, and GTPase-activating proteins. GEFs initiate the exchange of GDP with GTP and promote the association of Rho with its effector molecules.[6] Vasoconstrictors, including endothelin, angiotensin II, and urotensin II, induce VSMC contraction by activating RhoA via heterotrimeric GTP-binding protein-coupled receptors.[7,8] $G_{12/13}$ is responsible for this vasoconstrictor-mediated RhoA activation. The effectors of $G_{12/13}$, RGS (regulator for G protein signaling) domain- containing RhoGEF family members, p115RhoGEF, PDZ-RhoGEF, and LARG, have been identified as GEFs for RhoA.[9,10] Typical RhoGEF family members including RGS domain- containing RhoGEFs contain Dbl homology (DH) domains and pleckstrin homology (PH) domains. More than 60 RhoGEF family members containing DH-PH domains have been found in the human genome,[11] yet most of them have not been characterized to date.

Original received March 12, 2003; revision received May 2, 2003; accepted May 19, 2003.

From the Department of Structural Analysis (H.O., S.K., Y.K., M.M., N.M.), National Cardiovascular Center Research Institute, Suita, Osaka, Japan; the Department of Molecular and Cellular Pathology (H.S.), Hokkaido University, Sapporo, Japan.

Correspondence to Naoki Mochizuki, Department of Structural Analysis, National Cardiovascular Center Research Institute, Fujishirodai 5-7-1, Suita, Osaka 565-8565, Japan. E-mail nmochizu@ri.ncvc.go.jp

Circulation Research is available at http://www.circresaha.org

DOI: 10.1161/01.RES.0000079310.81429.C8

Eph family tyrosine kinase receptors consist of two groups: EphA group members respond to ephrin-A, which is anchored to the cell membrane by glycosylphosphatidylinositol, whereas EphB group members respond to ephrin-B, containing a transmembrane domain. Among them, only EphA4 can cross-respond to both ephrin-A and -B.[12] Recently, the Eph-ephrin system has been found to be involved in vascular development and also in mediating intracellular signaling in vascular endothelial cells in angiogenesis.[13–16]

We found that KIAA0915 was closely related to ephexin. Ephexin, which contains DH and PH domains, has been shown to bind to EphA4 and exhibit GEF activity for RhoA, Rac1, and Cdc42 in neuronal cells.[17] The DH and PH domains were conserved in KIAA0915, which we renamed Vsm-RhoGEF (vascular smooth muscle–specific RhoGEF), because it was expressed exclusively in VSMCs.

In this study, we investigated the function and the regulation of Vsm-RhoGEF in VSMCs. We demonstrate that Vsm-RhoGEF functions as a GEF for RhoA and that the GEF activity of Vsm-RhoGEF is regulated by the activation of EphA4 and the subsequent tyrosine phosphorylation of Vsm-RhoGEF. Collectively, our data suggest that the cell-cell contact-triggered ephrin-EphA4 interaction and the subsequent Vsm-RhoGEF activation may contribute to vascular contraction by regulating RhoA.

Materials and Methods

Reagents and Antibodies

Recombinant soluble mouse ephrin-A1-human Fc chimeric protein (ephrin-A1/Fc) was purchased from R&D Systems (Minneapolis, Minn). Ephrin-A1/Fc was prepared as described previously, and 1 μg/mL ephrin-A1/Fc chimera was used in the following experiments.[16] Protein A- and G-Sepharose were from Calbiochem (La Jolla, Calif). Anti-EphA4, anti-RhoA, and anti-Cdc42 antibodies were from Santa Cruz Biotechnology (Santa Cruz, Calif); anti-FLAG antibody was from Sigma-Aldrich (St Louis, Mo); rhodamine-phalloidin was from Molecular Probes (Eugene, Ore); anti-Rac1 was from Transduction Laboratories (Lexington, Ky); anti-HA antibody was from Roche Diagnostics (Basel, Switzerland); and anti-phosphotyrosine (PY100) antibody was from Cell Signaling Technology (Beverly, Mass). Anti-GFP (green fluorescent protein) was developed in our laboratory. Anti-Vsm-RhoGEF antibody was raised in rabbits against the synthetic peptide (EAVGPSSGTPNAPPP corresponding to the carboxy terminus of Vsm-RhoGEF) coupled to keyhole limpet hemacyanin.

Expression Plasmids

cDNA clone of Vsm-RhoGEF (KIAA0915) was obtained from Kazusa DNA Research Institute (Chiba, Japan). pCA-EGFP-Vsm-RhoGEF-WT, pCA-EGFP-Vsm-RhoGEF-DH-PH, and pCA-EGFP-Vsm-RhoGEF-PH were derived from pCAGGS eukaryotic expression vector and expressed enhanced green fluorescent protein (EGFP)-tagged wild type, DH-PH domains, and PH domain of Vsm-RhoGEF, respectively (Figure 1A).[18] pCXN2-FLAG-IRES-EGFP was derived from pCAGGS and contained an internal ribosome entry site (IRES) and the coding region of EGFP at the 3′ side.[19] The DNA fragments encoding full-length or PH domain of Vsm-RhoGEF were amplified by polymerase chain reaction (PCR) and subcloned into pCXN2-FLAG-IRES-EGFP vector. cDNA of RhoQL substituted at Gln63 for Leu was amplified by PCR and ligated into pCXN2 vector. pCXN2-Rac1V12 and pCXN2-FLAG-CdcV12 were obtained from M. Matsuda (Osaka University, Suita, Japan). pCI-HA-EphA4 expressing HA-tagged EphA4 was obtained from M. Tanaka (Hamamatsu University, Shizuoka, Japan). All of the DNA fragments amplified by PCR were ligated into pCR-BluntII-TOPO vector (Invitrogen, Carlsbad, Calif), and the sequence was confirmed with ABI Prism 3700 (Applied Biosystems Japan, Tokyo, Japan).

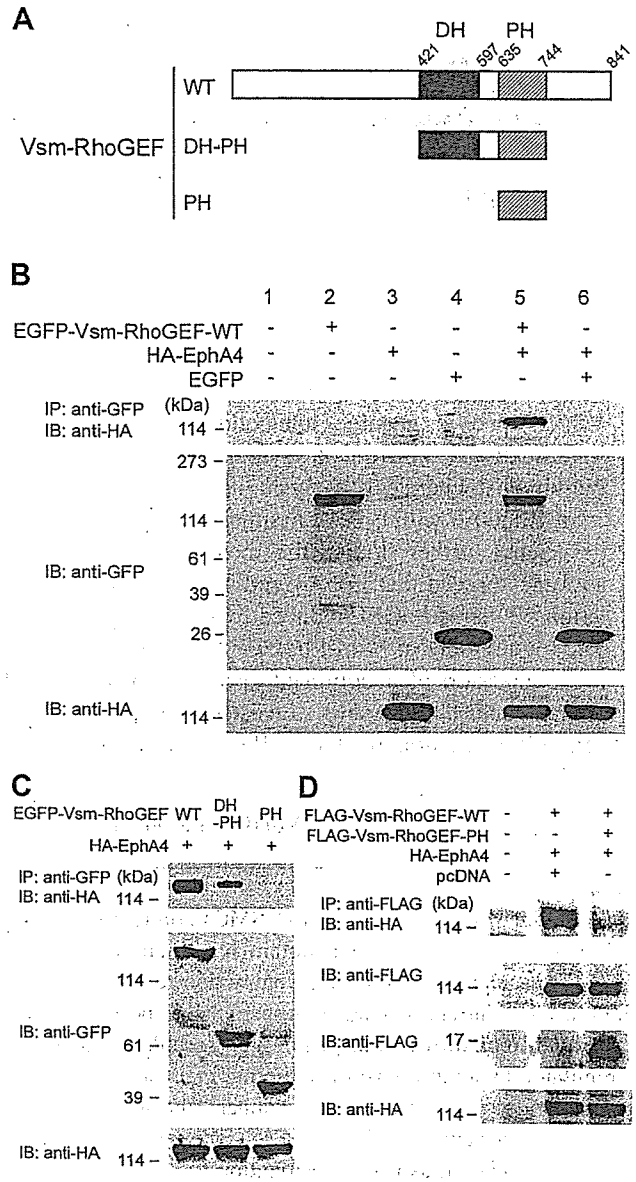

Figure 1. Association of Vsm-RhoGEF with EphA4. A, Schematic illustration of Vsm-RhoGEF and its truncated mutants. DH indicates Dbl homology domain, PH, pleckstrin homology domain. B, 293T cells were transfected with plasmids indicated at the top. Cell lysates were immunoprecipitated (IP) with anti-GFP and immunoblotted (IB) with anti-HA. C, 293T cells were transfected with plasmids as indicated at the top. The association of EGFP-tagged Vsm-RhoGEF and its deletion mutants with carboxy-terminally HA-tagged EphA4 was analyzed as in panel B. D, Cell lysates of 293T cells transfected with plasmids as indicated at the top were subjected to immunoprecipitation and immunoblotting with antibodies as indicated at the left. Note that overexpression of PH of Vsm-RhoGEF inhibits the association of Vsm-RhoGEF with EphA4. Immunoblot result is representative of those performed at least 3 times.

Cells and Transfection

Rat aortic smooth muscle cells (A7r5 cells) were purchased from American Type Culture Collection (Manassas, Va). Human coronary artery smooth muscle cells (HCASMCs) were from Cascade Biolog-

ics (Portland, Ore). HCASMCs were maintained in HuMedia-SG2 (Kurabo, Osaka, Japan) supplemented with a growth additive set as described previously.[19] 293T cells and A7r5 cells were cultured in DMEM (Invitrogen) supplemented with 10% FBS, 2 mmol/L L-glutamine and 15 mmol/L $NaHCO_3$. 293T cells were transfected by calcium phosphate method, and A7r5 cells were transfected by using LipofectAMINE 2000 reagent (Invitrogen). A7r5 cells were starved for more than 6 hours before the ephrin-A1/Fc stimulation in DMEM/F-12 (Invitrogen) without phenol red supplemented with 2 mmol/L L-glutamine, 10 mmol/L HEPES, 15 mmol/L $NaHCO_3$, and 0.5% bovine serum albumin fraction V.

Immunoprecipitation and Immunoblotting

Cells were washed with PBS three times and lysed in lysis buffer (150 mmol/L NaCl, 20 mmol/L Tris hydrochloride, pH 7.5, 1.5 mmol/L $MgCl_2$, 1 mmol/L Na_3VO_4, 1% Triton X-100, 10 mmol/L NaF, and protease inhibitor cocktail (Roche Applied Science). Lysates were precleared by centrifugation at 15 000*g* for 10 minutes, and immunoprecipitated by antibodies, indicated in the figure, and protein A- or G-Sepharose. Immunoprecipitates were subjected to SDS-PAGE and immunoblotting with antibodies as indicated in the figure. Protein isolation of each organ from Wister-Kyoto rats was performed according to the method as previously described.[20] Briefly, each organ from a rat was cleaned, pulverized in liquid nitrogen, and homogenated. Equivalent amounts of protein from each organ were separated on SDS-PAGE and transferred to PVDF membrane for immunoblotting with anti-Vsm-RhoGEF. Proteins reacting with primary antibodies were visualized by an enhanced chemiluminescence system (Amersham Biosciences UK, Buckinghamshire, UK) for detecting peroxidase-conjugated and species-matched secondary antibodies and analyzed with an LAS-1000 system (Fuji Film, Tokyo, Japan).

Immunohistochemical Analysis

Rats were sacrificed by overdose injection of pentobarbital intraperitoneally. The immunohistochemical study followed the protocol as described previously.[21] The formalin-fixed paraffin-embedded sections of rat organs were deparaffinized, heated by pressure cooker in 10 mmol/L sodium citrate pH 6.0 for 3 minutes for antigen unmasking, and cooled in water. After washing in 0.02% Tween-20/PBS, they were treated with 0.3% H_2O_2 methanol and normal goat serum to quench endogenous peroxidase activity and thereafter incubated with anti-Vsm-RhoGEF (1:1000) or anti-EphA4 (1:200) at 4°C overnight. After incubation with the biotinylated goat anti-rabbit IgG and peroxidase-labeled streptavidin, immunoreactive products were visualized by 3,3′-diaminobenzidine tetrahydrochloride. For comparison of immunostaining, counterstaining was also performed with hematoxylin. All animal procedures were performed according to the *Guide for the Care and Use of Laboratory Animals* (NIH, revision 1996).

Detection of GTP-Bound RhoA, Rac1, and Cdc42

GTP-bound RhoA, Rac1, and Cdc42 was detected by the pull-down assay as reported previously.[22,23] 293T cells transfected with the plasmids indicated in the figure or ephrin-A1/Fc–stimulated A7r5 cells were lysed in lysis buffer. Cleared lysates were incubated with glutathione *S*-transferase (GST)-Rho-binding domain of Rhotekin or GST-Rac/Cdc42 binding domain of PAK for Rac1 or Cdc42, respectively. GST-bound small GTPases collected on glutathione-agarose beads were subjected to SDS-PAGE followed by immunoblotting with anti-RhoA, anti-Rac1, or anti-Cdc42 antibody. Quantitative analyses of immunoblots were performed using Image Gauge version 3.4X software included in an LAS-1000 system. Relative intensity compared with the control was calculated and expressed as an average with standard deviation (SD). Statistically significant difference among each group was evaluated by the Student's *t* test.

Confocal Images

A7r5 cells transfected with plasmids indicated in the figure or stimulated with preclustered ephrin-A1/Fc for the indicated time were washed with PBS three times and fixed by 2% paraformalde-

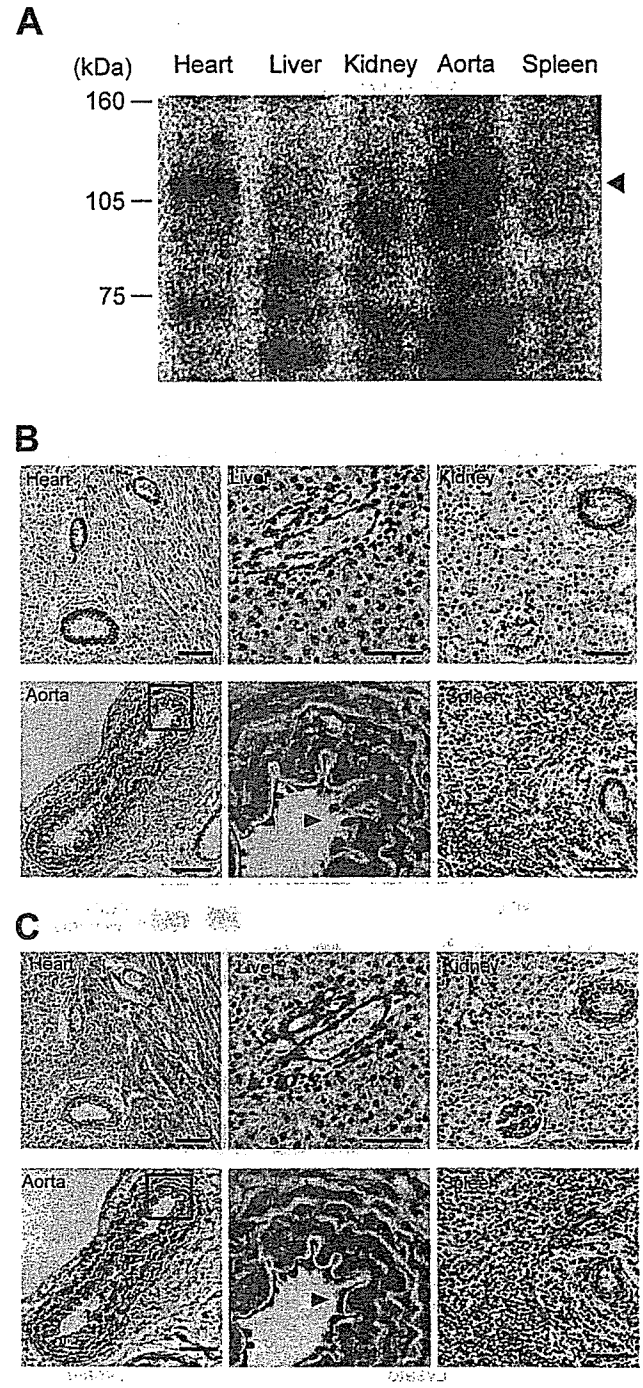

Figure 2. Vsm-RhoGEF is specifically expressed in vascular smooth muscle. A, Immunoblot analysis of tissue samples from rats with anti-RhoGEF antibody. Arrowhead indicates Vsm-RhoGEF. B, Immunohistochemical analysis of Vsm-RhoGEF in rat tissue section. Tissue sections from the organs as indicated in the top left corner were prepared and immunostained with anti-Vsm-RhoGEF antibody as described in Materials and Methods. Immunoreactivity was visualized by 3,3′-diaminobenzidine tetrahydrochloride (brown). The boxed region (bottom left) was enlarged (bottom middle). The arrowhead indicates that endothelial cells were negative for immunoreactivity to anti-Vsm-RhoGEF. C, Immunohistochemical analysis for EphA4 was performed as in panel B. Note that endothelial cells indicated by the arrowhead show positive immunoreaction to anti-EphA4. Bar=50 μm.

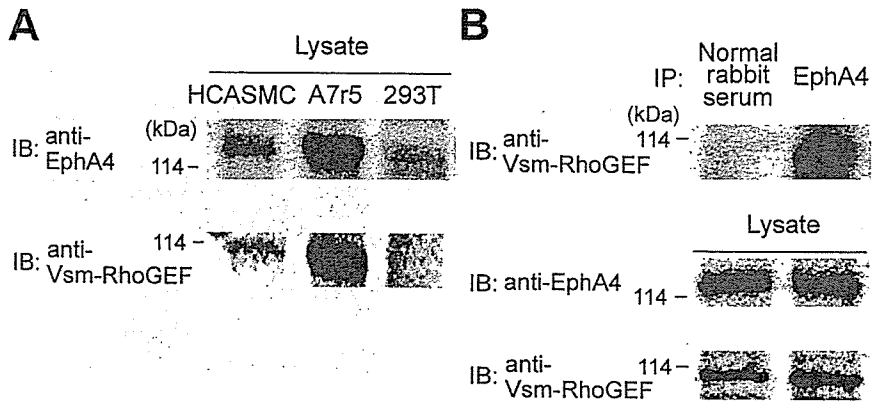

Figure 3. Vsm-RhoGEF is expressed and associated with EphA4 in VSMCs. A, Cell lysates of HCASMCs, A7r5 cells, and 293T cells were subjected to SDS-PAGE and immunoblot (IB) with antibodies as indicated at the left. B, Cell lysates of A7r5 cells were incubated (IP) with either normal rabbit serum or anti-EphA4, followed by SDS-PAGE and immunoblotting with anti-Vsm-RhoGEF. Cell lysates were analyzed for the expression of EphA4 (middle) and Vsm-RhoGEF (bottom).

hyde at room temperature for 30 minutes, followed by permeabilization with 0.05% Triton X-100 for 10 minutes. Permeabilized cells were incubated with rhodamine-phalloidin to detect actin filaments. Cells were imaged by a confocal microscope, BX50WI controlled by Fluoview (Olympus, Tokyo, Japan).

RNA Interference

Small, interfering RNAs (siRNA), 5′-AAGAUCAUUG-AGCGCUGCAGC-3′ and 5′-GCUGCAGCGCUCAAUGAU-CUU-3′ (Dharmacon Research, Lafayette, Colo) were annealed and introduced into A7r5 cells by using LipofectAMINE 2000 reagent (Invitrogen). The rat RNA sequence corresponding to human Vsm-RhoGEF was derived from a partial cDNA sequence we obtained by RT-PCR using a rat cDNA library as a template. Scrambled double-stranded RNA used as a negative control was also obtained from Dharmacon Research.

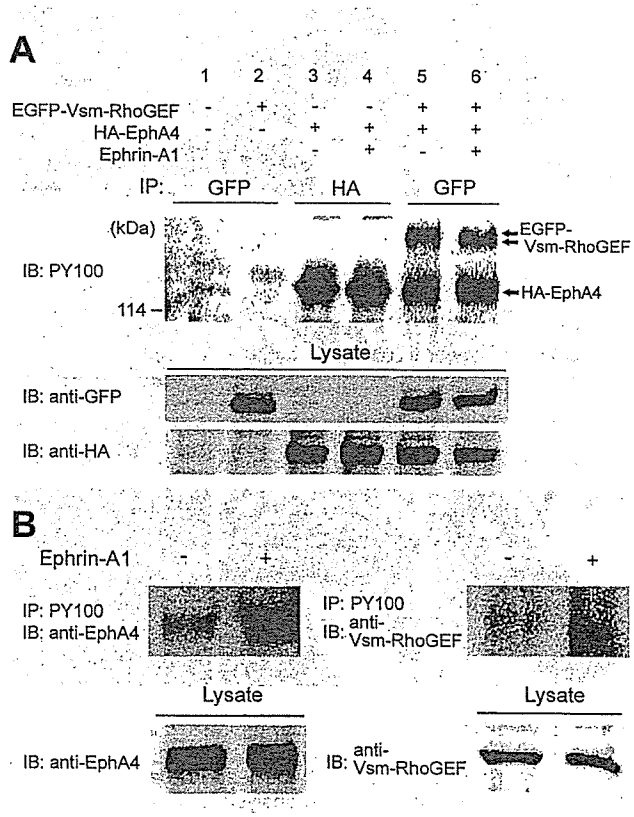

Figure 4. Phosphorylation of Vsm-RhoGEF depends on that of EphA4. A, 293T cells transfected with plasmids as indicated at the top were starved for 6 hours and stimulated (+) or unstimulated (−) with preclustered ephrin-A1/Fc. Cell lysates were incubated (IP) with antibodies as indicated and subjected to immunoblot with anti-phosphotyrosine antibody (PY100). Phosphorylated EphA4 and Vsm-RhoGEF are indicated by the arrow and double arrow, respectively. B, Phosphorylation of EphA4 and Vsm-RhoGEF were examined in the A7r5 cells stimulated without (−) or with (+) 1 μg/mL preclustered ephrin-A1/Fc. Cell lysates were immunoprecipitated with PY100, followed by immunoblotting with either anti-EphA4 (left) or anti-Vsm-RhoGEF (right).

Results

Vsm-RhoGEF Associates With EphA4

Vsm-RhoGEF (KIAA0915) is structurally related to ephexin, which associates with EphA4 in neuronal cells.[17] We thus tested whether Vsm-RhoGEF associated with EphA4. Schematic illustration of Vsm-RhoGEF and its truncated forms used for the following experiments is shown in Figure 1A. Carboxy-terminally HA-tagged EphA4 was coimmunoprecipitated with EGFP-tagged Vsm-RhoGEF in 293T cells expressing both proteins (Figure 1B, lane 5). EGFP used as a negative control did not coimmunoprecipitate with EphA4. Although we examined the association between Vsm-RhoGEF and EphB2, EphB2 receptors were not coimmunoprecipitated with EGFP-tagged Vsm-RhoGEF (data not shown). To examine the region required for the association with EphA4, we constructed truncated forms of Vsm-RhoGEF and examined whether these could associate with EphA4 in 293T cells. Full length, the DH-PH domains, or the PH domain of Vsm-RhoGEF were expressed in 293T cells with HA-tagged EphA4. We found that the EGFP-tagged tandem DH-PH domains were coimmunoprecipitated with EphA4, whereas PH domain alone was not coimmunoprecipitated with EphA4 (Figure 1C). These results suggest that the association between Vsm-RhoGEF and EphA4 requires either the DH or the DH/PH domains of Vsm-RhoGEF. To determine whether the PH domain is required for binding to EphA4, we tested whether overexpression of the PH domain of Vsm-RhoGEF inhibited the association of Vsm-RhoGEF with EphA4 (Figure 1D). PH domain perturbed the association of Vsm-RhoGEF with EphA4, indicating that both DH domain and PH domain are required for the association of Vsm-RhoGEF with EphA4.

Vsm-RhoGEF Is Coexpressed and Associated With EphA4 in Vascular Smooth Muscle

We proceeded to examine the tissue distribution of Vsm-RhoGEF and the localization of Vsm-RhoGEF by immuno-

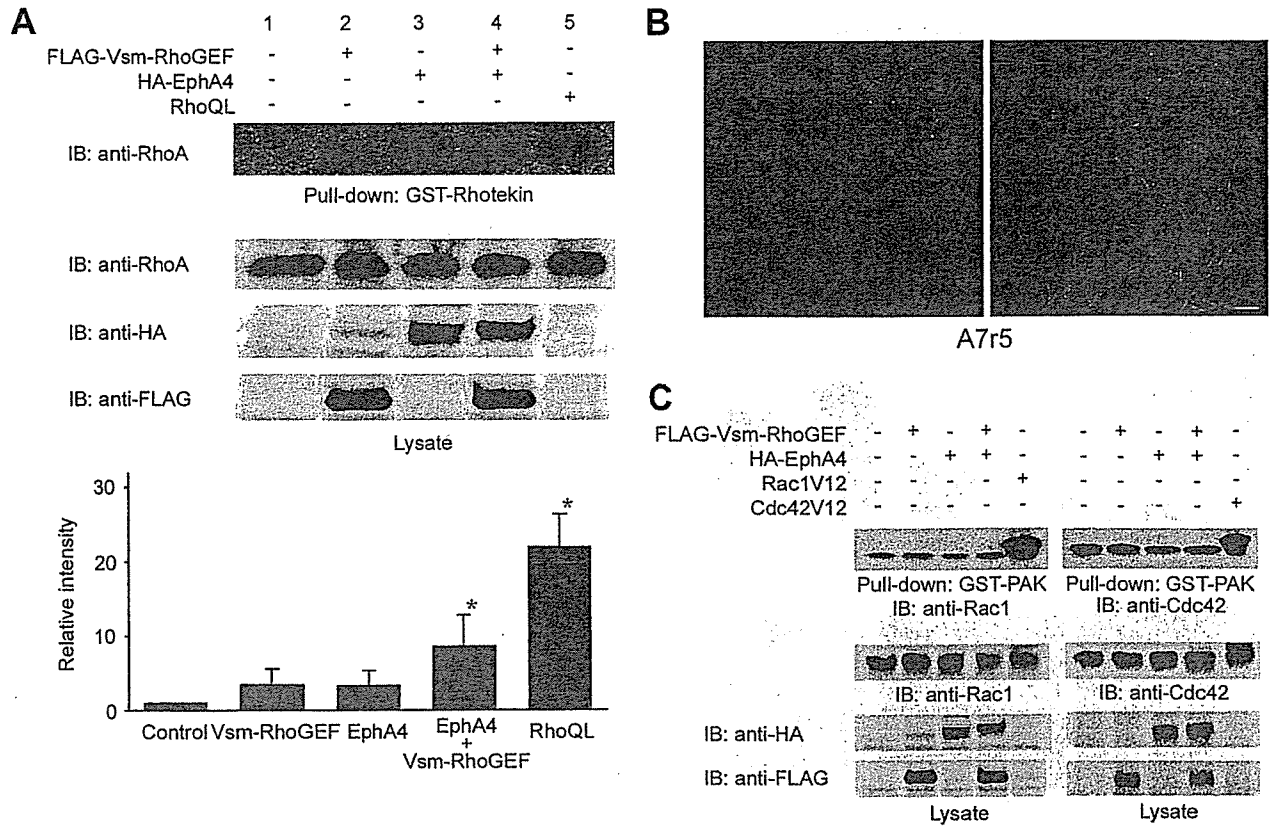

Figure 5. RhoA activation and induction of actin stress fiber by EphA4-Vsm-RhoGEF signaling. A, 293T cells were transfected with the plasmids as indicated at the top. Cell lysates were pulled down by GST-Rhotekin and subjected to immunoblot with anti-RhoA. GTP-bound RhoA was quantified by the intensity of the bands, analyzed by ImageGauge software included in LAS-1000 system (bottom). *Significant difference ($P<0.05$) compared with the control, determined by t test. B, A7r5 cells transfected with pCXN2-FLAG-Vsm-RhoGEF-IRES-EGFP were labeled with rhodamine-phalloidin to visualize actin stress fiber. Note that the cell expressing Vsm-RhoGEF marked by green fluorescence (green) exhibits an increase in bundling of actin stress fiber. Cells were imaged on a confocal microscope, BX50WI, controlled by Fluoview (Olympus). Bar=20 μm. C, GTP-bound Rac1 (left) and Cdc42 (right) were similarly analyzed as in panel A by pull-down assay using anti-Rac1 or anti-Cdc42 antibodies and GST-PAK instead of GST-Rhotekin.

histochemical analysis using an anti-Vsm-RhoGEF antibody developed in our laboratory. Proteins from rat tissues were separated by SDS-PAGE and analyzed by immunoblotting with anti-Vsm-RhoGEF antibody. Immunoreactive bands were detected in the samples obtained from the heart and the aorta at the expected size of Vsm-RhoGEF (Figure 2A). Immunohistochemical analysis using anti-Vsm-RhoGEF detected Vsm-RhoGEF in the vascular smooth muscle of all examined organs including heart, liver, kidney, aorta, and spleen (Figure 2B). The staining was specific for Vsm-RhoGEF since it was abolished by the preabsorption with the peptide used for the immunization (data not shown). Cardiomyocytes showed weak positive immunoreaction to anti-Vsm-RhoGEF, which was consistent with the immunoblot analysis (Figure 2A); however, other parenchymal cells or blood cells did not show any immunoreactivity. We further examined the expression of EphA4 using serial sections used in those examined for Vsm-RhoGEF expression (Figure 2C). Notably, EphA4 was similarly expressed in the vascular smooth muscle that expressed Vsm-RhoGEF. Furthermore, immunoreactivity for EphA4 was found in cardiomyocytes and glomeruli in the kidney. Vascular endothelium was immunopositive for EphA4 but not for Vsm-RhoGEF, as indicated by the arrowhead (Figures 2B and 2C, bottom middle panels). These results suggested that the EphA4-Vsm-RhoGEF complex may function in VSMCs.

To confirm the coexpression and association of Vsm-RhoGEF with EphA4, we performed coimmunoprecipitation experiments using VSMCs. Both HCASMCs and rat aortic smooth muscle cells expressed EphA4 and Vsm-RhoGEF, as shown by the immunoblots detecting endogenous EphA4 and Vsm-RhoGEF (Figure 3A). Neither EphA4 nor Vsm-RhoGEF was detected in 293T cells used as a negative control. Vsm-RhoGEF was coimmunoprecipitated by anti-EphA4 in A7r5 cells, but not by normal rabbit serum used as a negative control (Figure 3B), indicating that Vsm-RhoGEF associates with EphA4 in VSMCs.

Tyrosine Phosphorylation of Vsm-RhoGEF Is Induced by Activation of EphA4 Upon Ephrin-A1 Stimulation

To understand the molecular mechanism of Vsm-RhoGEF regulation by EphA4, we examined EphA4 activation–dependent tyrosine phosphorylation of Vsm-RhoGEF. HA-tagged EphA4 in 293T cells was autophosphorylated irrespective of preclustered ephrin-A1/Fc stimulation (Figure 4A, lanes 3 and 4, indicated by arrow). Furthermore, we found that

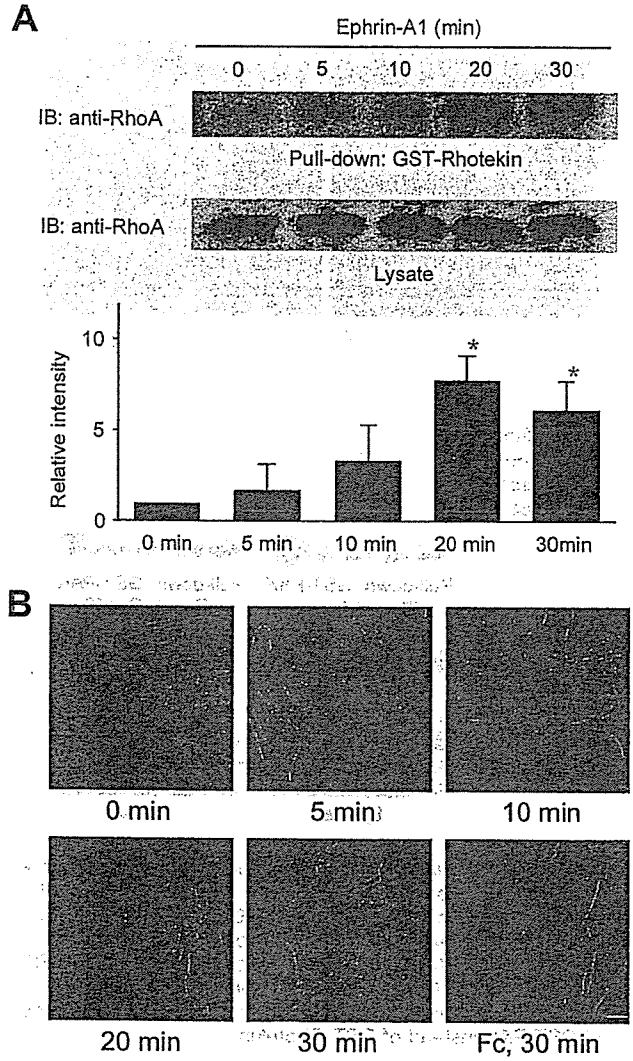

Figure 6. Ephrin-A1–induced RhoA activation and the assembly of actin stress fiber. A, Lysates of A7r5 cells stimulated with preclustered ephrin-A1/Fc for time indicated at the top were subjected to pull-down analysis for RhoA (top). GTP-bound RhoA was quantified by the intensity of the band on the immunoblot as analyzed in Figure 5A. *Significant difference ($P<0.05$) compared with the control. B, A7r5 cells were stimulated with preclustered ephrin-A1/Fc or Fc alone (Fc) for time as indicated at the bottom. Cells were fixed with 2% paraformaldehyde, permeabilized with 0.05% Triton X-100, and incubated with rhodamine-phalloidin to visualize actin stress fiber. Bar=20 μm.

EGFP-tagged Vsm-RhoGEF was phosphorylated on tyrosine residues when it was cotransfected with HA-tagged EphA4 (Figure 4A, lanes 5 and 6, indicated by double arrow). These data suggested that the tyrosine phosphorylation of Vsm-RhoGEF depends on that of EphA4. Thus, we tested whether phosphorylation of Vsm-RhoGEF is dependent on ephrin-A1–induced EphA4 phosphorylation in A7r5 cells. Both EphA4 and Vsm-RhoGEF were tyrosine-phosphorylated upon ephrin-A1 stimulation (Figure 4B).

EphA4 Activation Upon Ephrin-A1 Stimulation Induces RhoA Activation in VSMCs

The DH-PH–containing GEFs have guanine nucleotide exchange activity for members of the Rho family GTPases including Rho, Rac, and Cdc42. We expected that Vsm-RhoGEF would function as a GEF for RhoA, regulating actin–myosin II coupling, based on its specific expression in VSMCs. Indeed, when EphA4 and Vsm-RhoGEF were coexpressed in 293T cells, GTP-bound RhoA was increased, as demonstrated by pull-down assay using GST-Rhotekin (Figure 5A, lane 4). These results and the results shown in Figure 4A indicated that EphA4 phosphorylation induces the phosphorylation of Vsm-RhoGEF and enhance its GEF activity for RhoA.

We then tested whether Vsm-RhoGEF induces the assembly of actin stress fiber, which is a typical consequence of RhoA activation. A7r5 cells overexpressing Vsm-RhoGEF exhibited increased assembly of actin stress fibers compared with untransfected cells (Figure 5B). Moreover, we examined the guanine nucleotide exchange activity of Vsm-RhoGEF for Rac1 and Cdc42 by pull-down assay using GST-PAK (Figure 5C). Vsm-RhoGEF exhibited GEF activity for neither Rac1 nor Cdc42, indicating that Vsm-RhoGEF functions as a specific GEF for RhoA.

Ephrin-A1 Induces RhoA Activation in A7r5 Cells

To examine whether ephrin-A1 induces RhoA activation and the subsequent assembly of actin stress fibers, we stimulated A7r5 cells with preclustered ephrin-A1/Fc. GTP-bound RhoA was increased in a time-dependent manner, as shown in Figure 6A. This increase in GTP-bound RhoA reached a maximum at 20 minutes after ephrin-A1 stimulation (Figure 6A, top and bottom). These data indicate that Vsm-RhoGEF functions as a GEF for RhoA downstream of EphA4 when both EphA4 and Vsm-RhoGEF are phosphorylated upon ephrin-A1 stimulation (Figures 4B and 6A).

We further examined whether ephrin-A1 induced the assembly of actin stress fibers in A7r5 cells. Cells serum-starved for 6 hours were stimulated with preclustered ephrin-A1/Fc for the time indicated at the bottom of the figure. The most increased assembly of stress fibers was found 30 minutes after stimulation (Figure 6B, bottom middle panel). This prominent stress fiber formation followed the RhoA activation with an approximate 10-minute delay (Figures 6A and 6B).

Vsm-RhoGEF Is Required for Ephrin-A1–Induced Assembly of Actin Stress Fibers in A7r5 Cells

To investigate whether Vsm-RhoGEF is essential for ephrin-A1–induced actin stress fiber formation, we overexpressed the PH domain of Vsm-RhoGEF to inhibit the association of Vsm-RhoGEF with EphA4 (Figure 1D). A7r5 cells expressing the mutant marked by IRES-driven EGFP expression exhibited fewer actin stress fibers than untransfected cells before ephrin-A1 stimulation (Figure 7A, top). This reduction in stress fibers in cells transfected with a dominant-negative mutant remained unchanged in response to preclustered ephrin-A1/Fc (Figure 7A, bottom). These observations suggest that Vsm-RhoGEF is involved in the regulation of actin stress fiber formation even in unstimulated cells. In addition, we performed an RNA interference experiment to examine the effect of Vsm-RhoGEF on actin stress fiber and RhoA activation. A7r5 cells transfected with double-stranded small-